iScience

CellPress
OPEN ACCESS

Article

Streptavidin Promotes DNA Binding and Activation of cGAS to Enhance Innate Immunity

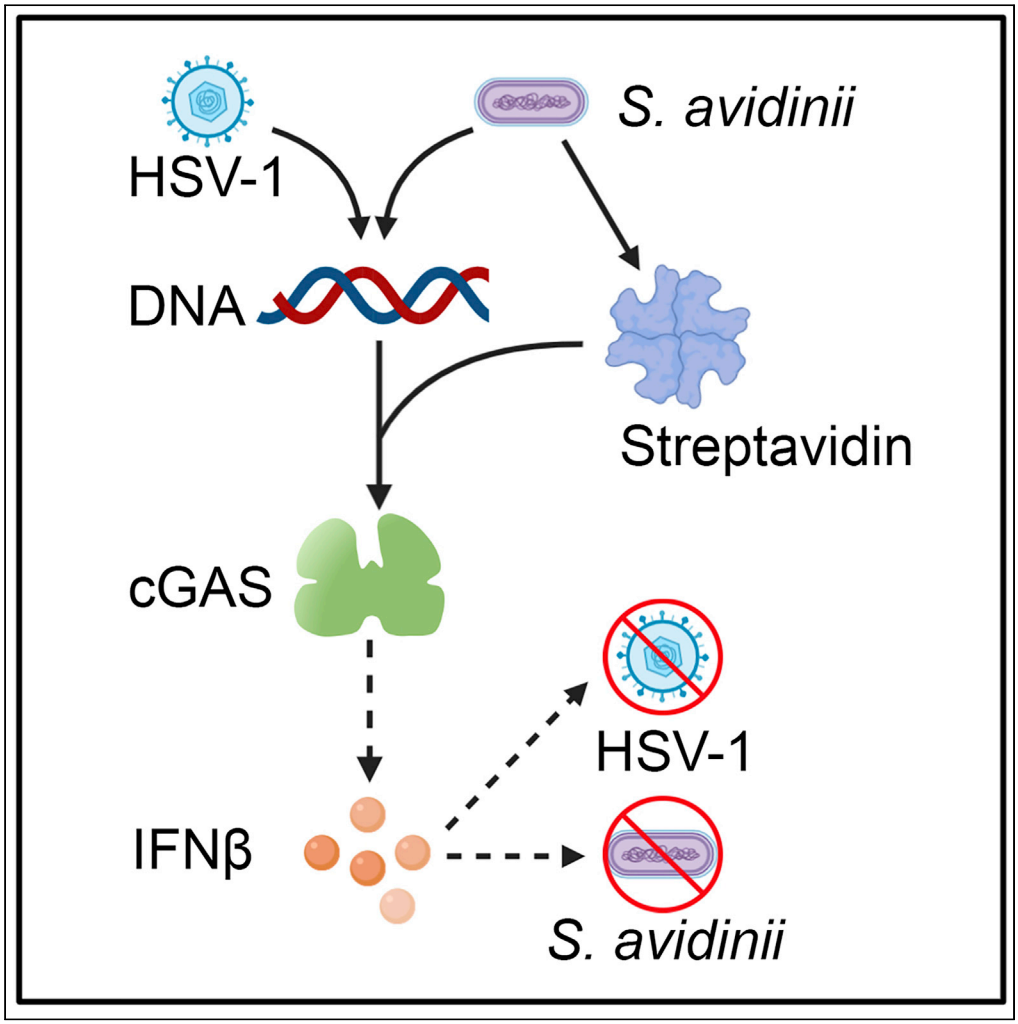

Yanqiong Zhang, Zhe Ma, Ying Wang, ..., Qi Zhang, Blossom Damania, Pengda Liu

blossom_damania@med.unc.edu (B.D.)
pengda_liu@med.unc.edu (P.L.)

HIGHLIGHTS

The bacterial protein streptavidin binds cGAS to promote cGAS activation

Streptavidin enhances cGAS binding to DNA and promotes cGAS phase separation

Streptavidin nanoparticles enhance HSV-1 induced innate immunity

These findings complicate clinical and biotechnological applications of streptavidin

Zhang et al., iScience *23*, 101463
September 25, 2020
https://doi.org/10.1016/j.isci.2020.101463

iScience

CellPress
OPEN ACCESS

Article

Streptavidin Promotes DNA Binding and Activation of cGAS to Enhance Innate Immunity

Yanqiong Zhang,[1,2,5] Zhe Ma,[1,5] Ying Wang,[1,2,5] Joshua Boyer,[2] Guoxin Ni,[1] Liang Cheng,[1,3] Siyuan Su,[1,2] Zhigang Zhang,[1] Zhichuan Zhu,[1,2] Jiayi Qian,[1,2] Lishan Su,[1,3] Qi Zhang,[2] Blossom Damania,[1,3,4,*] and Pengda Liu[1,2,6,*]

SUMMARY

cGAS/STING signaling plays an essential role in sensing cytosolic DNA. cGAS activity is regulated by posttranslational modifications and binding partners. cGAS interactome largely includes mammalian or viral proteins. Whether and how bacterial proteins bind cGAS to modulate innate immunity remain elusive. Here, we found streptavidin, a secreted bacterial protein, selectively bound cGAS to promote DNA-induced cGAS activation and interferon-β production. Mechanistically, streptavidin enhanced DNA binding and cGAS phase separation, therefore facilitating cGAS activation. Using an HSV-1-infected mouse model, we found streptavidin nanoparticles facilitated HSV-1 clearance through improving innate immunity. Considering the clinical usage of streptavidin as an immune stimulant and drug delivery vehicle and its biotechnological usage for biotin-labeled protein purification and detection, our studies not only provide an example for a bacterial protein regulating cGAS activity but also suggest caution needs to be taken when using streptavidin in various applications given to its ability to induce innate immunity.

INTRODUCTION

In mammals, the immune system contains both specific (adaptive immunity) and nonspecific immunity (innate immunity) to defend against pathogens. As the first line of host defense, the innate immune system utilizes germLine-encoded receptors named pattern recognition receptors (PRRs) to detect invading pathogens (Brubaker et al., 2015). As DNA or RNA is indispensable for propagation of pathogens, sensing of invading foreign RNA and DNA serves as a fundamental mechanism for host defense. Human cells respond to accumulated cytosolic DNA through activation of cGAS/STING signaling (Sun et al., 2013). Mechanistically, accumulated cytosolic DNA, from viral (Goubau et al., 2013) or bacterial (Patrick et al., 2016) infections, or intrinsic damaged mitochondria (Sliter et al., 2018) and genomic DNA (Bakhoum et al., 2018; Dou et al., 2017; Harding et al., 2017; Mackenzie et al., 2017), binds and activates mammalian cGAS (cGAMP synthase) to generate 2′3′-cGAMP that subsequently activates STING to promote type I interferon (IFN) production and expression of antiviral and immune modulatory genes (Diner et al., 2013; Li et al., 2013; Sun et al., 2013; Zhang et al., 2013). Mouse models suggest that loss of cGAS sensitizes mice to viral infection (Gao et al., 2013; Li et al., 2013), whereas hyperactivation of the cGAS/STING pathway results in autoimmune diseases (Gao et al., 2015) and radioresistance (Deng et al., 2014). Consistent with its role in innate immune recognition of DNA, cGAS/STING signaling also provides an anticancer function by which cGAS activation or administration of cGAMP synergistically functions with immune check blockades to suppress melanoma growth in murine models (Wang et al., 2017) (reviewed in (Ablasser and Chen, 2019) and (Barber, 2015)).

Beyond innate immunity, cGAS also regulates tumorigenic phenotypes. For example, cGAS is essential for cellular senescence (Yang et al., 2017), and chromosomal-instability-induced cGAS activation facilitates breast cancer metastasis (Bakhoum et al., 2018). In addition, nuclear cGAS binds PARP1 to suppress HR and promote lung cancer growth in a cGAS-enzyme-independent manner (Liu et al., 2018). Given its pivotal roles in both innate immunity and tumorigenesis, cGAS activity is tightly controlled. Various

[1]Lineberger Comprehensive Cancer Center, The University of North Carolina at Chapel Hill, Chapel Hill, NC 27599, USA

[2]Department of Biochemistry and Biophysics, The University of North Carolina at Chapel Hill, Chapel Hill, NC 27599, USA

[3]Department of Microbiology and Immunology, University of North Carolina at Chapel Hill, Chapel Hill, NC 27599, USA

[4]University of North Carolina Center for AIDS Research, University of North Carolina at Chapel Hill, Chapel Hill, NC 27599, USA

[5]These authors contributed equally

[6]Lead Contact

*Correspondence: blossom_damania@med.unc.edu (B.D.), pengda_liu@med.unc.edu (P.L.)

https://doi.org/10.1016/j.isci.2020.101463

posttranslational modifications have been reported to fine-tune cGAS activity and function, including phosphorylation (Liu et al., 2018; Seo et al., 2015), acetylation (Dai et al., 2019), glutamylation (Xia et al., 2016), sumoylation (Cui et al., 2017; Hu et al., 2016), ubiquitination (Chen and Chen, 2019; Seo et al., 2018), and others (Ablasser and Gulen, 2016). In addition, cellular localization of cGAS provides an additional layer of regulation governing spatial cGAS activation (Barnett et al., 2019). cGAS also recognizes HIV DNA in the nucleus (Lahaye et al., 2018), and the nuclear cGAS binds centromeric DNA (Gentili et al., 2019) and chromatin that suppresses DNA repair (Jiang et al., 2019). On the other hand, chromatin binding in the nucleus suppressed cGAS activity (Volkman et al., 2019). Mechanistically, cGAS is activated by DNA binding to its N-terminus or enzymatic domain that triggers cGAS phase separation (Du and Chen, 2018). Intriguingly, multiple cGAS-binding proteins have been identified with roles in either suppressing cGAS activity (such as Beclin-1 (Liang et al., 2014), OASL (Ghosh et al., 2019), a herpesvirus virion protein ORF52 (Wu et al., 2015), and a cytomegalovirus tegument protein pp65 (Biolatti et al., 2018)) or promoting cGAS activity (such as PQBP1 (Yoh et al., 2015), G3BP1 (Liu et al., 2019), and ZCCHC3 (Lian et al., 2018)). Notably, most of the identified cGAS-binding proteins are either mammalian proteins or viral proteins, and there are a limited number of bacterial proteins observed to facilitate cGAS activation, such as HU from *Listeria monocytogenes* that bends DNA to create favorable DNA conformations for cGAS recognition (Andreeva et al., 2017). Whether and how any bacterial proteins bind and regulate cGAS activation and innate immunity remain elusive.

Streptavidin is a secreted bacterial protein produced by the soil bacterium *Streptomyces avidinii* with a high affinity for biotin (vitamin B7). Due to its nature as one of the strongest noncovalent interactions, streptavidin has been extensively used in molecular biology and biotechnology for purification and detection of biotin-labeled proteins or nucleotides (Dundas et al., 2013) or as a tool to identify new drug targets (Bykhovski et al., 2013), as well as in clinics as immune stimulants (Weir et al., 2014) or as a drug delivery vehicle (Jain and Cheng, 2017) for biotin-labeled biomaterials. Whether streptavidin affects innate immunity remains unknown.

RESULTS

Streptavidin Binds cGAS *In Vitro* and in Cells

Surprisingly, we found that streptavidin-conjugated agarose beads displayed a strong ability to pull down bacterially purified full-length His-hcGAS (human cGAS) proteins *in vitro* (Figure 1A). This was not true for biotin-interacting neutravidin-conjugated agarose beads, nor commonly used glutathione, Flag-antibody-, HA-antibody-, or Myc-antibody-coupled agarose beads (Figures 1A, S1A, and S1B). Streptavidin binding to hcGAS was further confirmed by using streptavidin magnetic beads to exclude the possibility that agarose beads contribute to hcGAS interaction with streptavidin *in vitro* (Figures 1B, S1C, and S1D). In addition, benzonase nuclease treatment that digest nucleotides (both DNA and RNA) did not affect hcGAS binding to streptavidin *in vitro* (Figure S1E and S1F), suggesting that observed cGAS binding to streptavidin is not mediated by DNA or RNA. The binding affinity of His-hcGAS with streptavidin was ~1.3 μM *in vitro* determined by ITC analysis (Figure 1C). Considering the tetramer form of streptavidin and allowable errors in protein concentration calculation, roughly streptavidin binds hcGAS in a 1:1 ratio (Figure 1C). Moreover, streptavidin, but not neutravidin beads, were able to pull down ectopically expressed hcGAS from HEK293 cells (Figures 1D and S1G) in a cGAS-enzyme-activity-independent manner (Figures 1E and S1H). More importantly, streptavidin beads were able to pull down endogenous hcGAS but not STING nor TBK1 in MDA-MB-231 cells (Figure 1F). Ectopically expressed streptavidin in HEK293 cells co-migrated with (Figure 1G) and interacted with transfected hcGAS in cells (Figure 1H). Moreover, streptavidin, but not neutravidin beads, was able to pull down bacterially purified mcGAS (mouse cGAS) proteins *in vitro* (Figure S1I) and endogenous mcGAS from either 4T1 (Figure S1J) or B16 cells (Figure S1K). Together, these data suggest that streptavidin binds both hcGAS and mcGAS *in vitro* and in cells.

Compared with biotin, the larger size of cGAS may prevent it from fitting into the biotin-binding pocket of streptavidin (Figure S1L). Interestingly, a streptavidin mutant (N23A/S27D/S45A) deficient in binding biotin (Howarth et al., 2006) largely retained its binding with cGAS (Figure 1I). In addition, saturating streptavidin beads with biotin, although reduced binding with biotin-labeled H4 peptides, did not significantly affect streptavidin binding with cGAS *in vitro* (Figure 1J). Titrating in increasing doses of biotin also did not compete with cGAS to bind streptavidin beads *in vitro* (Figures S1M and S1N). These data suggest that cGAS may not compete with biotin to recognize the same motif of streptavidin.

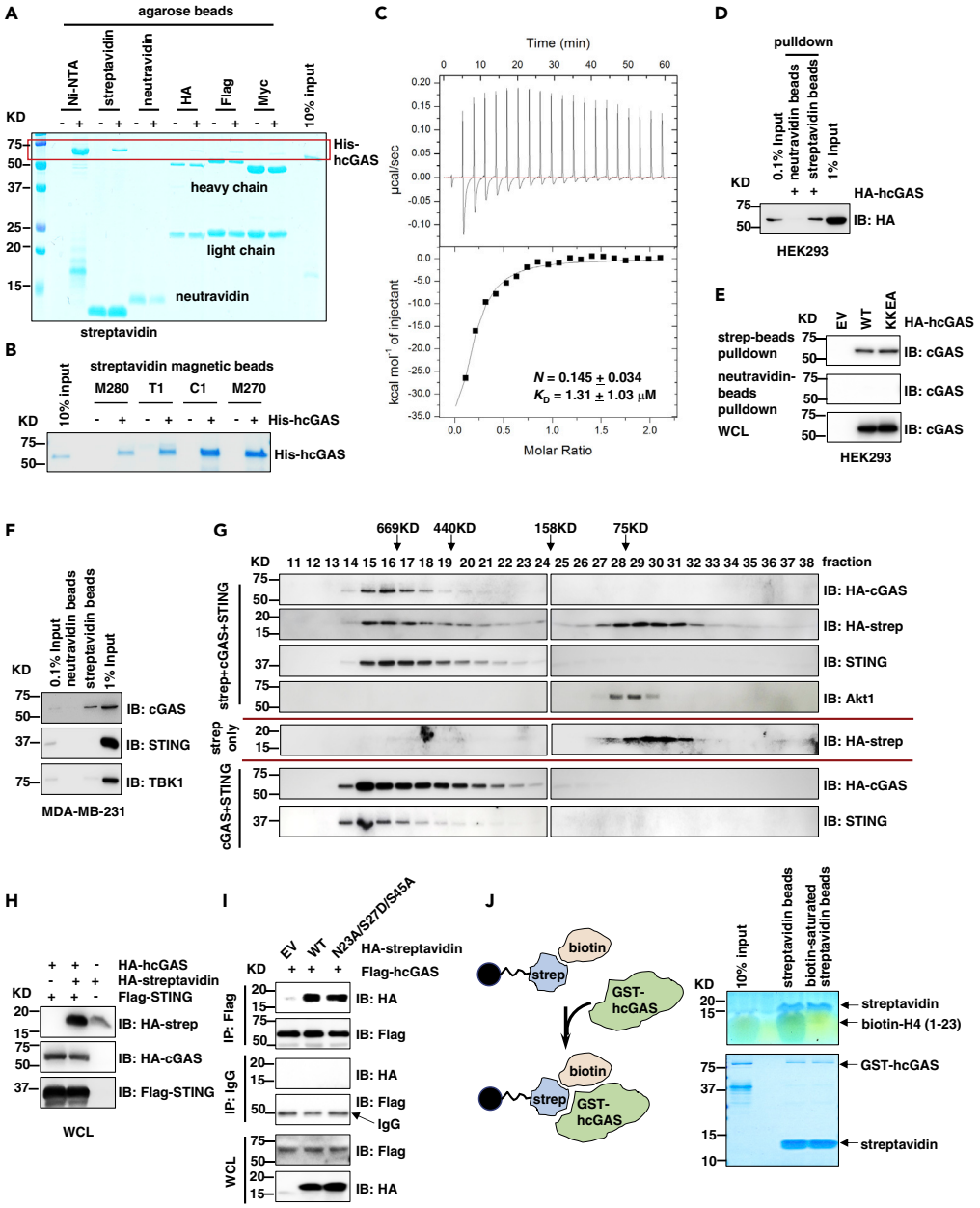

Figure 1. Streptavidin Directly Binds cGAS *In Vitro* and in Cells

(A and B) *In vitro* pull-down assays using indicated agarose beads (A) or magnetic beads (B) with recombinant His-hcGAS proteins demonstrate that streptavidin strongly interacts with cGAS. M280, T1, C1, and M270 are streptavidin magnetic beads from Invitrogen. Data represent results from two independent experiments.

(C) ITC analysis using bacterially purified His-hcGAS proteins and streptavidin proteins suggests their binding affinity of 1.2 μM *in vitro*.

(D and E) Streptavidin beads pull down hcGAS expressed in cells. Immunoblot (IB) analysis of whole cell lysates (WCL) and pulldowns by indicated beads derived from HEK293 cells transiently transfected with indicated hcGAS constructs. Notably, KKEA (K173E/R176E/K407E/K411A) is a cGAS mutant deficient in binding DNA. Data represent results from two independent experiments.

(F) IB analysis of streptavidin beads or neutravidin beads pulldowns using WCL derived from MDA-MB-231 cells. Forty-eight hours posttransfection, pull-down assays were performed. Data represent results from two independent experiments.

(G) A gel filtration experiment using cell lysates derived from HEK293 cells transfected with indicated DNA constructs.

(H) WCL of (G).

Figure 1. *Continued*

(I) IB analysis of IPs and WCL derived from HEK293T cells transfected with indicated DNA constructs. Cells were collected 48 h posttransfection. Data represent results from two independent experiments. N23A/S27D/S45A-streptavidin is a biotin binding deficient mutant.

(J) (Left panel) A cartoon illustration of the experimental procedure: streptavidin agarose beads were preincubated with excess amount of biotin at room temperature for 2 h and nonbinding biotin was washed off. Biotin-saturated and nonsaturated streptavidin beads were used to pull down biotin-H4 (1-23) peptides (top right panel) or recombinant GST-hcGAS proteins (top bottom panel). Data represent results from two independent experiments.

Streptavidin Binding Promotes cGAS Activation

Next, we examined if streptavidin binding to cGAS modulates cGAS activity. To this end, we generated EA.hy926 cells stably expressing either a GFP control or streptavidin (Figure S2A). We found that compared with GFP expressing EA.hy926 cells, streptavidin expression enhanced cellular TBK1-pS172 and IRF3-pS396 levels upon stimulation by ISD90 (Figure 2A) or ISD45 (Figure S2B) but not by the cGAS product, 2′3′-cGAMP (Figure 2B), and minimally affected these proteins upon RNA challenge with polyI:C (Figure S2C). As a result, streptavidin expression led to increased levels of IFNβ mRNA transcription (Figure 2C) and secreted IFNβ (Figures 2D and S2F). Notably, neither cGAS (Figure S2D) nor STING (Figure S2E) mRNA expression changes were observed under these treatments. These data suggest that streptavidin promotes DNA-induced cGAS activation and subsequent IFNβ production in cells. In addition, streptavidin was able to promote cGAS activation by either shorter ISD45 or longer ISD90 stimulation (Figure 2E). Given that streptavidin promotes cGAS activation at early ISD treatment time points, rather than sustains ISD90-induced TBK1 and IRF3 phosphorylation (Figure 2A), we further examined if streptavidin-enhanced innate immune activation depended on ISD90 concentrations. To this end, we found that under both 3 μg/mL and 6 μg/mL ISD90 stimulation conditions, expression of streptavidin enhanced IRF3-pS386 phosphorylation at early time points (Figures S2G and S2H). Moreover, to exclude possible effects of GFP as a negative control in modulating innate immune signaling, we engineered an empty vector (EV) expressing EA.hy926 cell line as an additional control. We found that compared with EV-expressing cells, streptavidin expression promoted TBK1/IRF3 phosphorylation and subsequent IFNβ production upon ISD90 (Figures S2I–S2K) but not under 2′3′cGAMP (Figures S2L–S2N) stimulation conditions, further supporting our conclusion that streptavidin binding to cGAS promotes cGAS activation. Interestingly, streptavidin itself was not able to activate STING in the absence of cGAS, and streptavidin also facilitated cGAS activation in HEK293T cells (Figure 2F), supporting the notion that streptavidin may function through cGAS to enhance DNA-induced innate immune responses. Notably, stable expression of streptavidin in EA.hy926 cells did not significantly affect cell growth (Figure S2O), revealing streptavidin-mediated cellular sensitivity to DNA insults is unlikely due to growth changes.

Streptavidin Enhances DNA Binding to cGAS to Facilitate cGAS Activation

Mechanistically, we found that both the N-terminus of cGAS (Figure S3A), a domain important for cGAS binding to DNA (Tao et al., 2017) and possible localization to plasma membrane (Barnett et al., 2019), and the C-terminal catalytic domain (ΔN) (Figures S3B–S3E) were necessary for binding streptavidin proteins *in vitro*. As a result, addition of recombinant streptavidin proteins only promoted DNA binding to the full-length hcGAS proteins (Figures 3A, 3B and S3F–S3G) but not N- (Figure 3C) nor ΔN-hcGAS proteins (Figure 3D) *in vitro*. Consistent with previous reports (Luecke et al., 2017), full-length or ΔN, but not the N-terminus of cGAS, was able to induce TBK1/IRF3 activation in cells (Figure S3H). Consistent with full-length cGAS being required for streptavidin binding, streptavidin only specifically promoted cGAS activation in cells expressing full-length, but not ΔN-cGAS (Figure S3I).

A "YRNA" Motif in Streptavidin Is Important for Streptavidin Binding to cGAS

Although distinct in primary protein sequence, avidin and streptavidin share common core structures for biotin binding. Interestingly, avidin is abundant in egg white with an additional glycoprotein portion compared with streptavidin; however, unlike streptavidin, avidin displayed minimal binding capacity with cGAS *in vitro* (Figures 3E and S3J). Coupled with the fact that a deglycosylated form of avidin, neutravidin, also did not bind cGAS *in vitro* (Figure 1A), these data suggest additional structural features in avidin and neutravidin prevent cGAS interaction and further suggest that cGAS may bind to a non-biotin-binding motif in streptavidin.

Intrigued by the fact that although both streptavidin and avidin share a similar structure to bind biotin, while unlike streptavidin, avidin does not bind cGAS (Figure 3E), we reasoned that unique structural

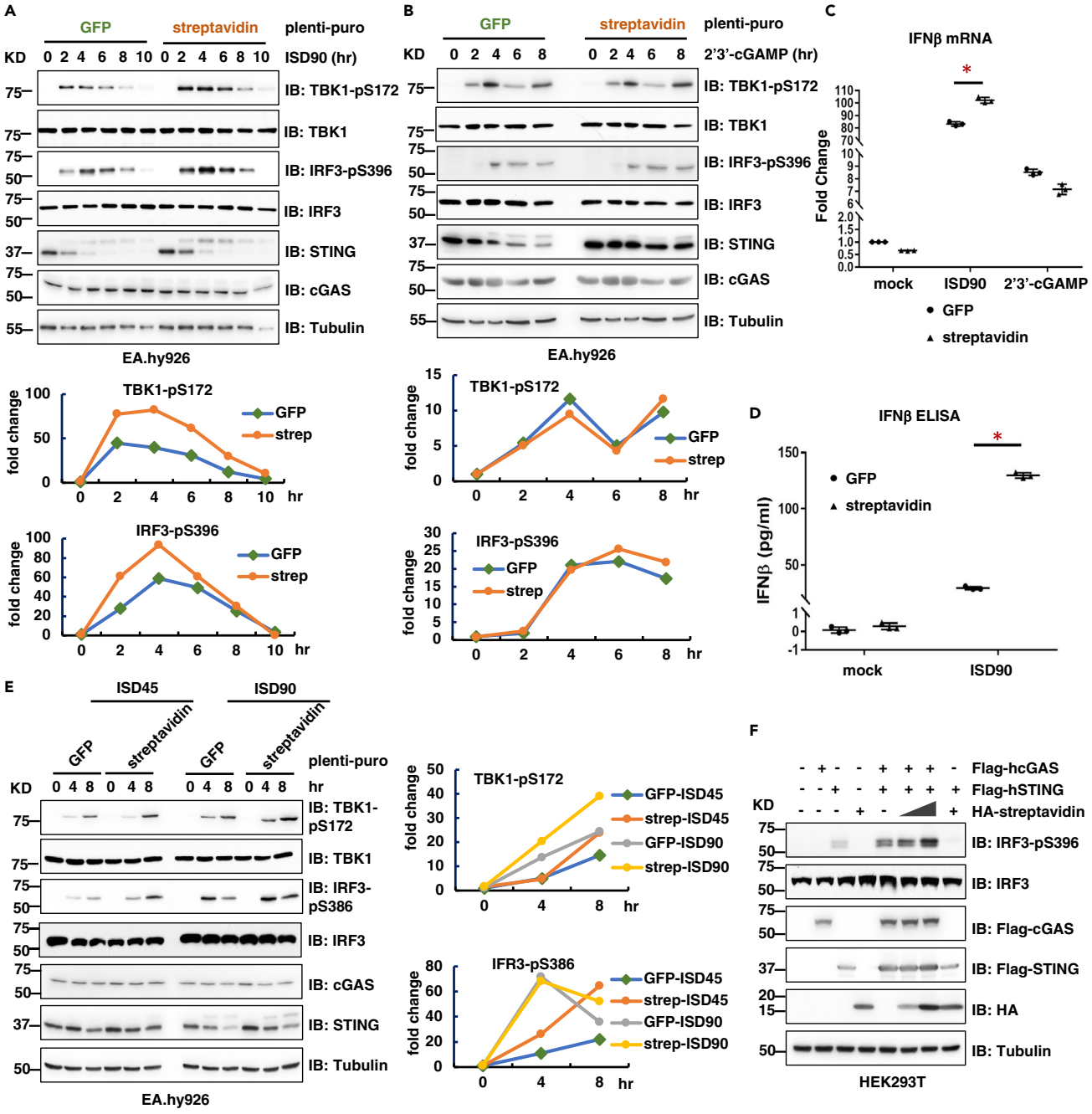

Figure 2. Streptavidin Binds cGAS to Facilitate cGAS Activation

(A and B) IB analysis of WCL derived from EA.hy926 cells stably expressing either GFP or streptavidin treated with 2 μg/mL ISD90 (A) or 5 μg/mL 2′3′-cGAMP (B) for indicated time periods. pTBK1 and pIRF3 signals were quantified by ImageJ and presented below each western blot. Data represent results from three independent experiments.

(C) RT-PCR analysis of IFNβ mRNA levels in EA.hy926 cells stably expressing either GFP or streptavidin treated with ISD90 or 2′3′-cGAMP for 6 h *$p < 0.05$ from Student's t tests. Data were obtained from biological triplicates.

(D) ELISA assays using cell culture media from EA.hy926 cells stably expressing either GFP or streptavidin treated with ISD90 for 16 h *$p < 0.05$ from Student's t tests. Data were obtained from biological triplicates.

(E) IB analysis of WCL derived from EA.hy926 cells stably expressing either GFP or streptavidin treated with ISD45 or ISD90 for indicated time periods. pTBK1 and pIRF3 signals were quantified by ImageJ and presented below each western blot. Data represent results from two independent experiments.

(F) IB analysis of WCL derived from HEK293T cells transfected with indicated DNA constructs. Cells were collected 48 h posttransfection. Data represent results from two independent experiments.

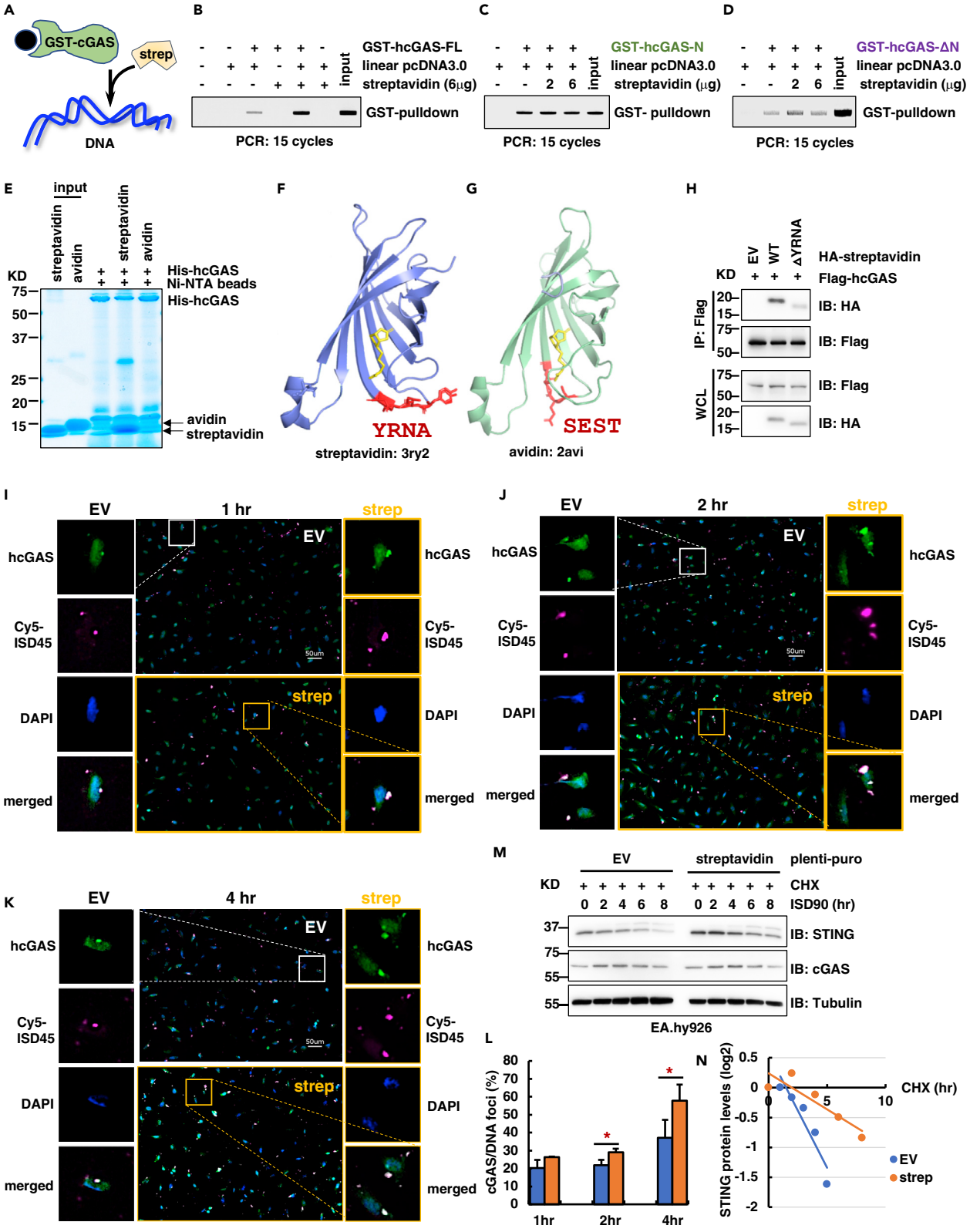
A
GST-cGAS
strep
DNA
B
GST-hcGAS-FL
linear pcDNA3.0
streptavidin (6μg)
input
GST-pulldown
PCR: 15 cycles
C
GST-hcGAS-N
linear pcDNA3.0
streptavidin (μg)
input
GST- pulldown
PCR: 15 cycles
D
GST-hcGAS-ΔN
linear pcDNA3.0
streptavidin (μg)
input
GST-pulldown
PCR: 15 cycles
E
input
streptavidin
avidin
KD
His-hcGAS
Ni-NTA beads
His-hcGAS
avidin
streptavidin
F
YRNA
streptavidin: 3ry2
G
SEST
avidin: 2avi
H
EV
WT
ΔYRNA
HA-streptavidin
Flag-hcGAS
KD
IP: Flag
IB: HA
IB: Flag
WCL
IB: Flag
IB: HA
I
EV
1 hr
strep
hcGAS
Cy5-ISD45
DAPI
merged
J
EV
2 hr
strep
hcGAS
Cy5-ISD45
DAPI
merged
K
EV
4 hr
strep
hcGAS
Cy5-ISD45
DAPI
merged
M
EV
streptavidin
plenti-puro
KD
CHX
ISD90 (hr)
IB: STING
IB: cGAS
IB: Tubulin
EA.hy926
L
cGAS/DNA foci (%)
1hr
2hr
4hr
N
STING protein levels (log2)
CHX (hr)
EV
strep

Figure 3. Streptavidin Binds cGAS to Enhance DNA Binding

(A) A cartoon illustration of the experimental design: recombinant GST-hcGAS proteins were immobilized onto glutathione (GSH) beads and incubated with linear pcDNA3.0 DNA in the presence or absence of streptavidin proteins.

(B–D) GST-hcGAS recombination proteins (including FL, full length in B, N-hcGAS in C, and ΔN-hcGAS in D) pull-down assays as described in (A) indicating streptavidin promotes full-length but not truncated cGAS binding to DNA *in vitro*. Where indicated, 15 cycles of PCR were used to determine DNA abundance from GST-hcGAS pulldowns. Data represent results from two independent experiments.

(E) His-hcGAS recombinant protein pull-down assays indicating hcGAS specifically binds streptavidin but not avidin *in vitro*. Data represent results from two independent experiments.

(F and G) Representative streptavidin protein structure (PDB: 3ry2) and avidin protein structure (PDB: 2avi) with the altered YRNA-streptavidin motif highlighted in red. Indicated protein structures were downloaded from PDB (protein database) and analyzed by PyMOL.

(H) IB analyses of Flag-IPs and WCL derived from HEK293T cells transfected with indicated DNA constructs. Cells were collected 48 h posttransfection. Data represent results from two independent experiments.

(I–K) Representative images from confocal imaging of EA.hy926 cells stably expressing either EV or streptavidin transfected with Cy3-ISD45 using a cGAS antibody at 1 h (I), 2 h (J), and 4 h (K) posttransfection. Scale bars represent 50 μm in I, J, and K.

(L) Quantification of colocalized cGAS/Cy3-DNA foci in I, J, and K. *$p < 0.05$ from Student's t tests. Quantifications were performed by counting at least 100 cells/each experiment and represent percentage of cells with puncta.

(M) A cycloheximide (CHX) chase experiment to measure endogenous STING protein half-life in EA.hy926 cells stably expressing either EV or streptavidin transfected with ISD90. Where indicated, 200 μg/mL CHX was added to cell culture and ISD90 was transfected into cells before taking time points. Data represent results from two independent experiments.

(N) Quantification of STING protein abundance in (M).

features in streptavidin contribute to streptavidin binding to cGAS. Through a primary protein sequence alignment between streptavidin and avidin (Figure S3K), we identified a "YRNA" motif that is missing in avidin and displays an extended structure in streptavidin (Figures 3F and 3G). Excitingly, deleting this "YRNA" motif disrupted streptavidin binding to cGAS (Figure 3H) and subsequently reduced DNA-induced activation of the cGAS/STING signaling (Figure S3L) in cells. In addition, YRNA deletion did not significantly affect streptavidin binding to biotin (-tagged histone peptides) *in vitro* (Figure S3M), further supporting that cGAS and biotin independently recognize streptavidin. Together, these data support that the "YRNA" motif in streptavidin plays an important role in bridging streptavidin binding to cGAS.

Streptavidin Enhances DNA Binding to cGAS to Promote cGAS Phase Separation

We found that streptavidin partially enhanced cGAS phase separation *in vitro*, which is necessary for cGAS activation (Du and Chen, 2018) induced by ISD45 (Figures S3N and S3O) or ISD90 (Figure S3P). In addition, streptavidin expression in cells significantly increased the number of cGAS puncta (indicators of cGAS activation) formed in cells upon ISD45 (Figures S3Q and S3R) or ISD90 stimulation (Figures S3S and S3T), which is presumably due to increased cGAS phase separation induced by streptavidin in a time-dependent dynamic manner (Figures 3I–3L). Overall, our data suggest that streptavidin directly binds cGAS to facilitate cGAS binding to DNA for activation. Intriguingly, we observed that STING expression levels were increased in streptavidin expressing EA.hy926 cells and upon ISD90 stimulation, streptavidin expression partially protected STING from degradation (Figures 3M and 3N), which was largely through attenuating STING ubiquitination-mediated STING degradation (Figure S3U). Given that streptavidin does not directly bind STING (Figure 1F), this observation suggests that streptavidin may have additional binding partners in indirectly regulating STING protein stability (eg, through regulating STING ubiquitination or STING binding with lysosomal components). Nevertheless, streptavidin may promote cGAS/STING activation in multiple ways.

Streptomyces avidinii Triggers Innate Immune Responses in Mice

As a soil bacterium, to date no report shows *S avidinii* as a potential human or animal pathogen to trigger innate immunity. Given that streptavidin is largely produced by *S avidinii*, we were curious to test if *S avidinii* could infect mice. We injected increasing doses of *S avidinii* via an IP route into C57BL/6 mice, and 24 h later mouse spleens were harvested. We found that 10×10^5 pfu of *S avidinii* triggered the increased innate immune response in C57BL/6 mice (compared with 10×10^3 and 10×10^7 pfu), as evidenced by increased TBK1-pS172 signals (Figure 4A) and IFNβ mRNA levels (Figures S4A and S4B). However, *S avidinii*-induced increase in pTBK1 was not only mediated by the cGAS/STING signaling pathway, given that in an *in vitro* co-culture model using *S avidinii* and MDA-MB-231 cells, *but* also promoted significant TBK1 phosphorylation in *cGAS*$^{-/-}$ MDA-MB231 cells, compared with wild-type (WT)-MDA-MB-231 cells (Figures 4B and S4C). It is plausible that in addition to DNA, bacterial proteins and RNA could also modulate innate immune responses through innate immune pathways such as endosomal Toll-like receptors and RIG-I/MAVS signaling, respectively (Ni et al., 2018; Tan et al., 2018). Notably, co-culture with *S avidinii* caused toxicity largely to WT but not *cGAS*$^{-/-}$ MDA-MB-231 cells *in vitro* (Figures 4C and S4D). This suggests that

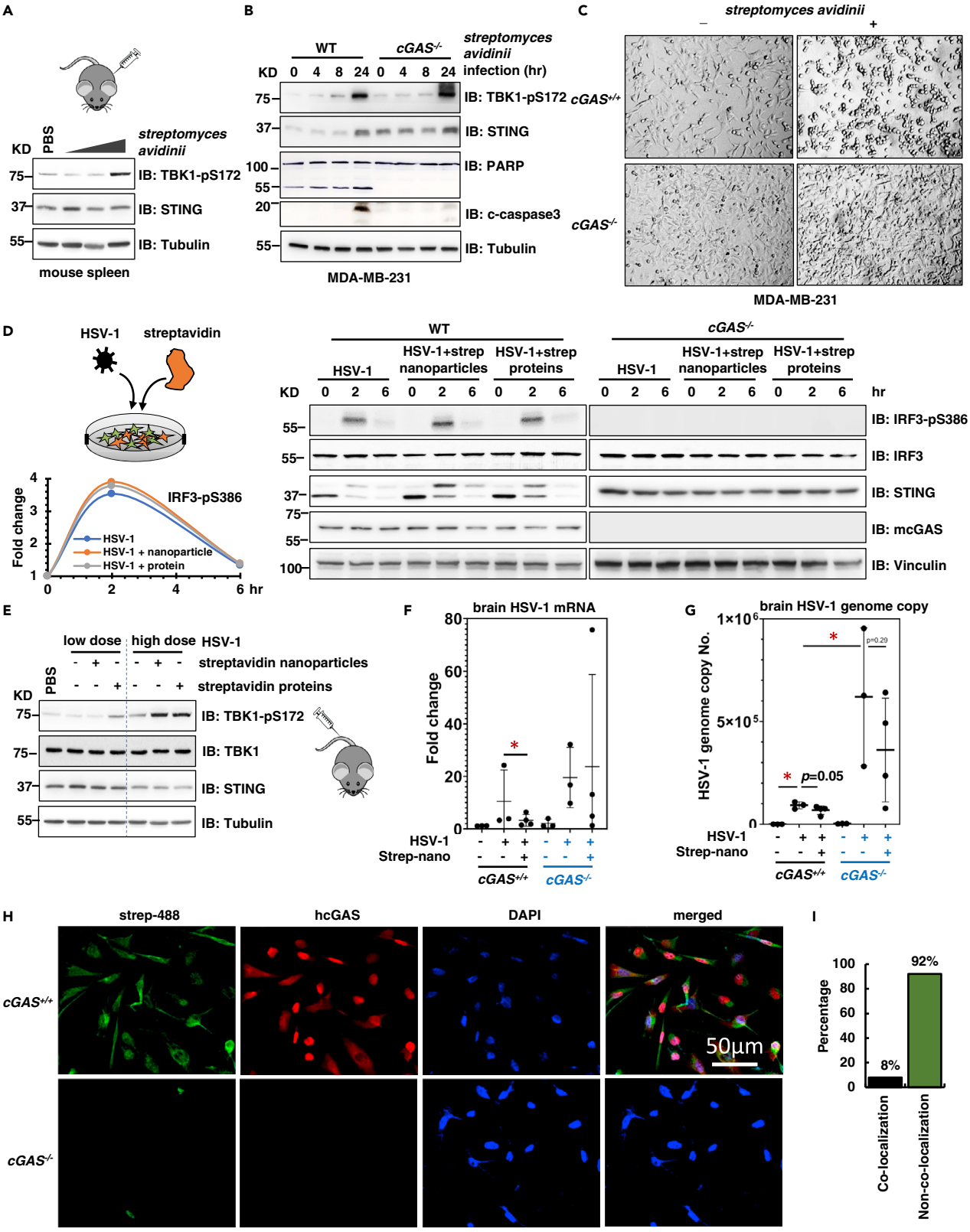
A
KD
PBS
streptomyces avidinii
75
IB: TBK1-pS172
37
IB: STING
55
IB: Tubulin
mouse spleen
B
WT
cGAS-/-
streptomyces avidinii infection (hr)
KD 0 4 8 24 0 4 8 24
75
IB: TBK1-pS172
37
IB: STING
100
55
IB: PARP
20
IB: c-caspase3
55
IB: Tubulin
MDA-MB-231
C
streptomyces avidinii
–
+
cGAS+/+
cGAS-/-
MDA-MB-231
D
HSV-1
streptavidin
Fold change
IRF3-pS386
HSV-1
HSV-1 + nanoparticle
HSV-1 + protein
0 2 4 6 hr
WT
cGAS-/-
HSV-1
HSV-1+strep nanoparticles
HSV-1+strep proteins
KD 0 2 6 0 2 6 0 2 6 0 2 6 0 2 6 0 2 6 hr
55
IB: IRF3-pS386
55
IB: IRF3
37
IB: STING
75
55
IB: mcGAS
100
IB: Vinculin
E
low dose
high dose
HSV-1
streptavidin nanoparticles
streptavidin proteins
PBS
KD
75
IB: TBK1-pS172
75
IB: TBK1
37
IB: STING
55
IB: Tubulin
F
brain HSV-1 mRNA
Fold change
80
60
40
20
0
*
HSV-1
Strep-nano
cGAS+/+
cGAS-/-
G
brain HSV-1 genome copy
HSV-1 genome copy No.
1×10^6
5×10^5
0
*
p=0.29
*
p=0.05
HSV-1
Strep-nano
cGAS+/+
cGAS-/-
H
strep-488
hcGAS
DAPI
merged
cGAS+/+
cGAS-/-
50μm
I
Percentage
100
80
60
40
20
0
8%
92%
Co-localization
Non-co-localization

Figure 4. Fluorescence-Conjugated Streptavidin or Avidin Detects Endogenous cGAS

(A) PBS or 10 × 10^3, 10 × 10^5, and 10 × 10^7 *S avidinii* bacteria were injected into BL6 mice through IP injection. Twenty-four hours postinjection mouse spleens were harvested and lysed for IB analyses.

(B) 10 × 10^7 *S avidinii* bacteria were co-cultured with WT or *cGAS*$^{-/-}$ MDA-MB-231 cells, and WCLs were obtained at indicated periods for IB analyses. Data represent results from two independent experiments.

(C) Representative images of cells from (B).

(D) 10 × 10^3.5 HSV-1 were used to infect WT or *cGAS*$^{-/-}$ MDA-MB-231 cells in the presence or absence of 20 μL streptavidin nanoparticles and 100 μg streptavidin proteins in 24-well plates. WCLs were obtained at indicated periods for IB analyses. Quantifications of IRF3-pS386 signals were performed by ImageJ. Data represent results from two independent experiments.

(E) A low dose (10 × 10^4 pfu) or a high dose (10 × 10^7 pfu) of HSV-1 was injected into BL6 mice through tail vein injection. Fifty microliters of streptavidin nanoparticles or 50 μg streptavidin proteins were co-injected where indicated. Twenty-four hours postinjection, mouse spleens were harvested for IB analyses.

(F) HSV-1 mRNA analyses using brain tissues from either WT or *cGAS*$^{-/-}$ BL6 mice with indicated treatments for 24 h *$p < 0.05$ from Student's t tests.

(G) HSV-1 genome copy number analyses using brain tissues from either WT or *cGAS*$^{-/-}$ BL6 mice with indicated treatments for 24 h. *$p < 0.05$ from Student's t tests.

(H) Representative images from confocal imaging of either *cGAS*$^{+/+}$ or *cGAS*$^{-/-}$ MDA-MB-231 cells using a fluorescence-labeled streptavidin probe (488-strep). The scale bar represents 50 μm.

(I) Quantification of (H). At least 100 cells were counted for each group for quantification.

cGAS-mediated IFNβ and other cytokine production might be important to trigger cellular apoptosis, as evidenced by cleaved-PARP and cleaved-caspase 3 signals (Figure 4B). In addition, we recognize that a streptavidin-negative strain will help further evaluate the specific effects of streptavidin on modulating innate immunity; however, due to technical difficulties we could not obtain such a strain and this will be a subject of future investigation. Based on these observations, we decided to examine if streptavidin nanoparticles, or streptavidin proteins, instead of *S avidinii*, promote DNA-induced innate immune signaling in both *in vitro* and *in vivo* models.

To this end, we used the DNA virus HSV-1 that has been well characterized to induce cGAS/STING signaling activation (Ni et al., 2018; Reinert et al., 2016). We found that infection of MDA-MB-231 cells with HSV-1 triggered cGAS/STING signaling activation and that addition of either streptavidin nanoparticles or streptavidin proteins facilitated HSV-1-induced IRF3 phosphorylation, which was largely dependent on cGAS (Figure 4D). Furthermore, we found that higher titers of HSV-1 led to increased cGAS activation (as evidenced by TBK1-pS172 signals) in spleens of C57BL/6 mice harvested 24 h postinfection (Figure 4E). Furthermore, co-administration of either streptavidin nanoparticles or streptavidin proteins through tail-vein injection further augmented TBK1-pS172 signals (Figure 4E). These data support that streptavidin facilitates cGAS activation upon HSV-1 infection *in vitro* and in mice. To further investigate if streptavidin also facilitates innate immune activation to clear HSV-1 infection, we injected a high dose of HSV-1 (1 × 10 × 10^8 pfu) into both WT and *cGAS*$^{-/-}$ C57BL/6 mice, in the presence or absence of streptavidin nanoparticles. We observed that cGAS was necessary for HSV-1-infection-induced TBK1 and IRF3 phosphorylation in mice (Figure S4E) and HSV-1-infected mice were sicker with significantly less movement and dramatically reduced body temperature. However, when co-injected with streptavidin nanoparticles, mice displayed a higher body temperature and increased movement. Twenty-four hours postinfection, brains were harvested for analyses on HSV-1 infection. We found that injection with streptavidin nanoparticles reduced HSV-1 mRNA expression in brains from WT but not *cGAS*$^{-/-}$ mice infected with HSV-1 (Figure 4F). In addition, HSV-1 genome copy number was also slightly reduced in streptavidin-nanoparticle-treated mice (Figure 4G). Together, these data suggest that streptavidin nanoparticles may help HSV-1 clearance, presumably due to promoting activation of the cGAS/STING signaling pathway. This is consistent with the immune stimulant function of streptavidin observed previously (Weir et al., 2014). However, we recognize that the protective effects from streptavidin proteins or streptavidin nanoparticles are minor, which might be due to low sequence homology between mouse and human cGAS. Although both hcGAS (Figure 1A) and mcGAS (Figure S1I) proteins bound to streptavidin *in vitro*, whether streptavidin recognizes and modulates hcGAS and mcGAS differently requires further in-depth investigations.

Fluorescent-Conjugated Streptavidin Probes Detect Endogenous cGAS Expression

Fluorescent-labeled streptavidin (Alex Fluor 488-strep) has been widely used in biotechnology to amplify the signal magnitude for *in vivo* labeling and detection of a given protein/nucleotide target by imaging (Howarth and Ting, 2008). Given our observation that streptavidin binds cGAS *in vitro* and in cells, we further tested if the streptavidin Fluor probes cross-react with endogenous cGAS. Using both WT and *cGAS*$^{-/-}$ MDA-MB-231 cells, we found that although streptavidin Fluor probes detected signals in *cGAS*$^{-/-}$ cells, which are presumably

biotin or other streptavidin-binding proteins, the presence of endogenous cGAS significantly enhanced signals generated by these probes (Figures 4H and S4F). These data suggest that streptavidin Fluor conjugates detect background signals including endogenous cGAS. Interestingly, staining endogenous cGAS by either a cGAS antibody or the streptavidin-488 probe resulted in largely noncolocalization of these two signals (Figure 4I), with streptavidin Fluor conjugates recognizing largely cytoplasmic cGAS species while the cGAS antibody detecting nuclear cGAS. Querying the information for this cGAS antibody (Cell Signaling Technology #15102) indicated that this antibody was generated using a cGAS peptide centered on Ala19 residue, which suggests that either the cGAS antibody and the streptavidin-488 probe recognize a similar motif in the N-terminus of cGAS or binding of either of them can cause a cGAS protein conformational change that is not favored by the other. To further examine if streptavidin has a preference for binding cytosolic cGAS, we fractionated BPH1 or EA.hy926 cells into both cytoplasmic and nuclear fractions (where cGAS was observed in both fractions) and subsequently performed streptavidin-agarose-beads-mediated pull-down assays. We found streptavidin agarose beads preferred cytoplasmic cGAS to nuclear cGAS for binding (Figures S4G–S4J). This could be due to differential posttranslational modifications on cytoplasmic or nuclear cGAS or because additional binding partners contribute to the observed binding preferences.

DISCUSSION

S avidinii is a soil bacterium, and it is not currently known whether it is a human or animal pathogen. We found that injecting *S avidinii* into C57BL/6 mice led to the induction of innate immunity (Figure 4A), suggesting that *S avidinii* may be a pathogenic bacterium. *S avidinii* is famous for its ability to produce and secrete streptavidin. Due to the tight and selective interactions with biotin even under stringent conditions, streptavidin and its homologs are widely used in protein detection, labeling, immune stimulation, and drug delivery (Dundas et al., 2013). Specifically, streptavidin is used to detect and purify strep-tagged or biotin-labeled proteins or other molecules such as DNA. Our immunostaining using a Fluor-labeled streptavidin in MDA-MB-231 cells (Figure 4H) indicates that streptavidin is capable of detecting endogenous cGAS proteins and therefore use of streptavidin in cellular immune assays may be problematic. In addition, streptavidin has been used as an immune stimulant to enhance efficacy of tumor vaccines with unknown mechanism (Weir et al., 2014), and various streptavidin-immune modulator fusions have shown enhanced immune regulatory effects (Arribillaga et al., 2013). Our data suggest that streptavidin activates innate immunity by facilitating cGAS activation induced by HSV-1 infection *in vitro* (Figure 4D) and in mice (Figure 4E). Moreover, streptavidin-coated nanoparticles are used in delivering biomaterials including antibodies, RNAs, DNAs, and compounds labeled with biotin (D'Agata et al., 2017), as well as pretargeted immunotherapy to deliver radiation only to cancerous cells due to the strong cell adsorptive ability of streptavidin (Altai et al., 2017). Due to the ability of streptavidin in activating innate immunity through cGAS, we speculate that streptavidin nanoparticles used in either drug delivery or pretargeted immunotherapy would trigger innate immune responses to enhance effects of these therapies. However, whether this effect is streptavidin dose dependent requires additional validations *in vivo*.

Notably, through a streptavidin protein sequence homology search, we found that streptavidin-like proteins are present in other soil bacterial species including *Actinokineospora spp.*, *Kitasatospora sp.*, *Pseudonocardia hispaniensis sp.*, *Saccharomonospora marina*, *Hymenobacter sp.*, and others. Streptavidin-like proteins are also present in sea creatures such as corals and sponges (Figure S4K). These proteins are uncharacterized but share significant sequence homology with streptavidin (Figure S4L). These observations suggest that these streptavidin-like bacterial proteins and coral/sponge proteins may exert similar function as streptavidin in not only binding biotin but also inducing innate immune responses through interacting with cGAS, which warrants further in-depth investigations.

Limitations of the Study

Although expression of streptavidin in mammalian cells facilitated DNA-induced cGAS activation, it remains critical to further validate if streptavidin directly enhances cGAS activity *in vitro* in the presence of DNA and if the cGAS catalytic domain is sufficient for this regulation. Moreover, it is important to further determine the stoichiometry of streptavidin proteins internalized by mammalian cells in a *S avidinii* infection model and if these internalized streptavidin proteins would enhance DNA-induced cGAS activation *in vivo* without significantly affecting cGAS cellular localization. Endogenous biotin is a co-factor for five human carboxylases and modulates gene expression through biotinylating histones (Zempleni et al., 2009). Given that streptavidin presumably depletes cellular biotin pools, effects from loss of biotin function should also be accounted for in the streptavidin-mediated cGAS pathway regulation. On the other hand, this suggests that using biotin-deficient streptavidin (eg. N23A/S27D/S45A)-coated nanoparticles may

provide advantages for *in vivo* applications. Our study raises the possibility that the soil bacterium *S avidinii* is recognized by the innate immune system as a foreign pathogen. However, relevant animal infection models are necessary for further validation.

Resource Availability

Lead Contact

Further information and requests for resources and reagents should be directed to and will be fulfilled by the Lead Contact, Pengda Liu (pengda_liu@med.unc.edu).

Materials Availability

Reagents generated in this study will be available upon request.

Data and Code Availability

The data that support the findings of this study are available from the corresponding authors (B.D. and P.L.) upon reasonable request.

METHODS

All methods can be found in the accompanying Transparent Methods supplemental file.

SUPPLEMENTAL INFORMATION

Supplemental Information can be found online at https://doi.org/10.1016/j.isci.2020.101463.

ACKNOWLEDGMENTS

We thank Liu and Damania lab members for critical reading of the manuscript and helpful discussions and thank Dr. Wesley Legant and Tim Austin Daugird for help with microscopy work. We also sincerely thank Dr. Zhijian James Chen for helpful advice. This work was supported by the NIH grants (R21CA234979 to P.L., 1K99CA230178 to Z.M., and DE028211 and CA239583 to B.D.), the V Scholar Research Grant (V2018-009, P.L.), the NCBC Flash Grant (P.L.), the Breast Cancer Alliance Young Investigator Grant (P.L.), and the UNC University Cancer Research Fund (P.L.). This work was partially supported by the National Cancer Institute of the National Institutes of Health under award number P30CA016086. The content is solely the responsibility of the authors and does not necessarily represent the official views of the National Institutes of Health.

AUTHOR CONTRIBUTIONS

Conceptualization, Y.Z., Z.M., B.D., Q.Z., and P.L.; Formal Analysis, Y.Z., Z.M., and Y.W.; Investigation, Y.Z., Z.M., Y.W., J.B., G.N., L.C., S.S., Z.Z., Z.Z., and J.Q.; Writing-Original Draft and Review& Editing, Y.Z., B.D., and P.L.; Visualization, Y.Z., Z.M., Y.W., and P.L.; Supervision, Q.Z., L, S., B.D., and P.L.; Funding Acquisition, Z.M., B.D., and P.L.

DECLARATION OF INTERESTS

The authors declare no competing interests.

Received: June 21, 2019
Revised: June 15, 2020
Accepted: August 12, 2020
Published: September 25, 2020

REFERENCES

Ablasser, A., and Chen, Z.J. (2019). cGAS in action: expanding roles in immunity and inflammation. Science *363*, eaat8657.

Ablasser, A., and Gulen, M.F. (2016). The role of cGAS in innate immunity and beyond. J. Mol. Med. (Berl.) *94*, 1085–1093.

Altai, M., Membreno, R., Cook, B., Tolmachev, V., and Zeglis, B.M. (2017). Pretargeted imaging and therapy. J. Nucl. Med. *58*, 1553–1559.

Andreeva, L., Hiller, B., Kostrewa, D., Lassig, C., de Oliveira Mann, C.C., Jan Drexler, D., Maiser, A., Gaidt, M., Leonhardt, H., Hornung, V., et al. (2017). cGAS senses long and HMGB/TFAM-bound U-turn DNA by forming protein-DNA ladders. Nature *549*, 394–398.

Arribillaga, L., Durantez, M., Lozano, T., Rudilla, F., Rehberger, F., Casares, N., Villanueva, L., Martinez, M., Gorraiz, M., Borras-Cuesta, F., et al. (2013). A fusion protein between streptavidin and the endogenous TLR4 ligand EDA targets

biotinylated antigens to dendritic cells and induces T cell responses in vivo. Biomed. Res. Int. *2013*, 864720.

Bakhoum, S.F., Ngo, B., Laughney, A.M., Cavallo, J.A., Murphy, C.J., Ly, P., Shah, P., Sriram, R.K., Watkins, T.B.K., Taunk, N.K., et al. (2018). Chromosomal instability drives metastasis through a cytosolic DNA response. Nature *553*, 467–472.

Barber, G.N. (2015). STING: infection, inflammation and cancer. Nat. Rev. Immunol. *15*, 760–770.

Barnett, K.C., Coronas-Serna, J.M., Zhou, W., Ernandes, M.J., Cao, A., Kranzusch, P.J., and Kagan, J.C. (2019). Phosphoinositide interactions position cGAS at the plasma membrane to ensure efficient distinction between self- and viral DNA. Cell *176*, 1432–1446.e11.

Biolatti, M., Dell'Oste, V., Pautasso, S., Gugliesi, F., von Einem, J., Krapp, C., Jakobsen, M.R., Borgogna, C., Gariglio, M., De Andrea, M., et al. (2018). Human cytomegalovirus tegument protein pp65 (pUL83) dampens type I interferon production by inactivating the DNA sensor cGAS without affecting STING. J. Virol. *92*, e01774-17.

Brubaker, S.W., Bonham, K.S., Zanoni, I., and Kagan, J.C. (2015). Innate immune pattern recognition: a cell biological perspective. Annu. Rev. Immunol. *33*, 257–290.

Bykhovski, A., Zhang, W., Jensen, J., and Woolard, D. (2013). Analysis of electronic structure, binding, and vibrations in biotin-streptavidin complexes based on density functional theory and molecular mechanics. J. Phys. Chem. B *117*, 25–37.

Chen, X., and Chen, Y. (2019). Ubiquitination of cGAS by TRAF6 regulates anti-DNA viral innate immune responses. Biochem. Biophys. Res. Commun. *514*, 659–664.

Cui, Y., Yu, H., Zheng, X., Peng, R., Wang, Q., Zhou, Y., Wang, R., Wang, J., Qu, B., Shen, N., et al. (2017). SENP7 potentiates cGAS activation by relieving SUMO-mediated inhibition of cytosolic DNA sensing. PLoS Pathog. *13*, e1006156.

D'Agata, R., Palladino, P., and Spoto, G. (2017). Streptavidin-coated gold nanoparticles: critical role of oligonucleotides on stability and fractal aggregation. Beilstein J. Nanotechnol. *8*, 1–11.

Dai, J., Huang, Y.J., He, X., Zhao, M., Wang, X., Liu, Z.S., Xue, W., Cai, H., Zhan, X.Y., Huang, S.Y., et al. (2019). Acetylation blocks cGAS activity and inhibits self-DNA-induced autoimmunity. Cell *176*, 1447–1460.e14.

Deng, L., Liang, H., Xu, M., Yang, X., Burnette, B., Arina, A., Li, X.D., Mauceri, H., Beckett, M., Darga, T., et al. (2014). STING-dependent cytosolic DNA sensing promotes radiation-induced type I interferon-dependent antitumor immunity in immunogenic tumors. Immunity *41*, 843–852.

Diner, E.J., Burdette, D.L., Wilson, S.C., Monroe, K.M., Kellenberger, C.A., Hyodo, M., Hayakawa, Y., Hammond, M.C., and Vance, R.E. (2013). The innate immune DNA sensor cGAS produces a noncanonical cyclic dinucleotide that activates human STING. Cell Rep. *3*, 1355–1361.

Dou, Z., Ghosh, K., Vizioli, M.G., Zhu, J., Sen, P., Wangensteen, K.J., Simithy, J., Lan, Y., Lin, Y., Zhou, Z., et al. (2017). Cytoplasmic chromatin triggers inflammation in senescence and cancer. Nature *550*, 402–406.

Du, M., and Chen, Z.J. (2018). DNA-induced liquid phase condensation of cGAS activates innate immune signaling. Science *361*, 704–709.

Dundas, C.M., Demonte, D., and Park, S. (2013). Streptavidin-biotin technology: improvements and innovations in chemical and biological applications. Appl. Microbiol. Biotechnol. *97*, 9343–9353.

Gao, D., Wu, J., Wu, Y.T., Du, F., Aroh, C., Yan, N., Sun, L., and Chen, Z.J. (2013). Cyclic GMP-AMP synthase is an innate immune sensor of HIV and other retroviruses. Science *341*, 903–906.

Gao, D., Li, T., Li, X.D., Chen, X., Li, Q.Z., Wight-Carter, M., and Chen, Z.J. (2015). Activation of cyclic GMP-AMP synthase by self-DNA causes autoimmune diseases. Proc. Natl. Acad. Sci. U S A *112*, E5699–E5705.

Gentili, M., Lahaye, X., Nadalin, F., Nader, G.P.F., Lombardi, E.P., Herve, S., De Silva, N.S., Rookhuizen, D.C., Zueva, E., Goudot, C., et al. (2019). The N-terminal domain of cGAS determines preferential association with centromeric DNA and innate immune activation in the nucleus. Cell Rep. *26*, 3798.

Ghosh, A., Shao, L., Sampath, P., Zhao, B., Patel, N.V., Zhu, J., Behl, B., Parise, R.A., Beumer, J.H., O'Sullivan, R.J., et al. (2019). Oligoadenylate-synthetase-family protein OASL inhibits activity of the DNA sensor cGAS during DNA virus infection to limit interferon production. Immunity *50*, 51–63.e5.

Goubau, D., Deddouche, S., and Reis e Sousa, C. (2013). Cytosolic sensing of viruses. Immunity *38*, 855–869.

Harding, S.M., Benci, J.L., Irianto, J., Discher, D.E., Minn, A.J., and Greenberg, R.A. (2017). Mitotic progression following DNA damage enables pattern recognition within micronuclei. Nature *548*, 466–470.

Howarth, M., Chinnapen, D.J., Gerrow, K., Dorrestein, P.C., Grandy, M.R., Kelleher, N.L., El-Husseini, A., and Ting, A.Y. (2006). A monovalent streptavidin with a single femtomolar biotin binding site. Nat. Methods *3*, 267–273.

Howarth, M., and Ting, A.Y. (2008). Imaging proteins in live mammalian cells with biotin ligase and monovalent streptavidin. Nat. Protoc. *3*, 534–545.

Hu, M.M., Yang, Q., Xie, X.Q., Liao, C.Y., Lin, H., Liu, T.T., Yin, L., and Shu, H.B. (2016). Sumoylation promotes the stability of the DNA sensor cGAS and the adaptor STING to regulate the kinetics of response to DNA virus. Immunity *45*, 555–569.

Jain, A., and Cheng, K. (2017). The principles and applications of avidin-based nanoparticles in drug delivery and diagnosis. J. Control. Release *245*, 27–40.

Jiang, H., Xue, X., Panda, S., Kawale, A., Hooy, R.M., Liang, F., Sohn, J., Sung, P., and Gekara, N.O. (2019). Chromatin-bound cGAS is an inhibitor of DNA repair and hence accelerates genome destabilization and cell death. EMBO J. *38*, e102718.

Lahaye, X., Gentili, M., Silvin, A., Conrad, C., Picard, L., Jouve, M., Zueva, E., Maurin, M., Nadalin, F., Knott, G.J., et al. (2018). NONO detects the nuclear HIV capsid to promote cGAS-mediated innate immune activation. Cell *175*, 488–501.e22.

Li, X.D., Wu, J., Gao, D., Wang, H., Sun, L., and Chen, Z.J. (2013). Pivotal roles of cGAS-cGAMP signaling in antiviral defense and immune adjuvant effects. Science *341*, 1390–1394.

Lian, H., Wei, J., Zang, R., Ye, W., Yang, Q., Zhang, X.N., Chen, Y.D., Fu, Y.Z., Hu, M.M., Lei, C.Q., et al. (2018). ZCCHC3 is a co-sensor of cGAS for dsDNA recognition in innate immune response. Nat. Commun. *9*, 3349.

Liang, Q., Seo, G.J., Choi, Y.J., Kwak, M.J., Ge, J., Rodgers, M.A., Shi, M., Leslie, B.J., Hopfner, K.P., Ha, T., et al. (2014). Crosstalk between the cGAS DNA sensor and Beclin-1 autophagy protein shapes innate antimicrobial immune responses. Cell Host Microbe *15*, 228–238.

Liu, H., Zhang, H., Wu, X., Ma, D., Wu, J., Wang, L., Jiang, Y., Fei, Y., Zhu, C., Tan, R., et al. (2018). Nuclear cGAS suppresses DNA repair and promotes tumorigenesis. Nature *563*, 131–136.

Liu, Z.S., Cai, H., Xue, W., Wang, M., Xia, T., Li, W.J., Xing, J.Q., Zhao, M., Huang, Y.J., Chen, S., et al. (2019). G3BP1 promotes DNA binding and activation of cGAS. Nat. Immunol. *20*, 18–28.

Luecke, S., Holleufer, A., Christensen, M.H., Jonsson, K.L., Boni, G.A., Sorensen, L.K., Johannsen, M., Jakobsen, M.R., Hartmann, R., and Paludan, S.R. (2017). cGAS is activated by DNA in a length-dependent manner. EMBO Rep. *18*, 1707–1715.

Mackenzie, K.J., Carroll, P., Martin, C.A., Murina, O., Fluteau, A., Simpson, D.J., Olova, N., Sutcliffe, H., Rainger, J.K., Leitch, A., et al. (2017). cGAS surveillance of micronuclei links genome instability to innate immunity. Nature *548*, 461–465.

Ni, G., Ma, Z., and Damania, B. (2018). cGAS and STING: at the intersection of DNA and RNA virus-sensing networks. PLoS Pathog. *14*, e1007148.

Patrick, K.L., Bell, S.L., and Watson, R.O. (2016). For better or worse: cytosolic DNA sensing during intracellular bacterial infection induces potent innate immune responses. J. Mol. Biol. *428*, 3372–3386.

Reinert, L.S., Lopusna, K., Winther, H., Sun, C., Thomsen, M.K., Nandakumar, R., Mogensen, T.H., Meyer, M., Vaegter, C., Nyengaard, J.R., et al. (2016). Sensing of HSV-1 by the cGAS-STING pathway in microglia orchestrates antiviral defence in the CNS. Nat. Commun. *7*, 13348.

Seo, G.J., Yang, A., Tan, B., Kim, S., Liang, Q., Choi, Y., Yuan, W., Feng, P., Park, H.S., and Jung, J.U. (2015). Akt kinase-mediated checkpoint of cGAS DNA sensing pathway. Cell Rep. *13*, 440–449.

Seo, G.J., Kim, C., Shin, W.J., Sklan, E.H., Eoh, H., and Jung, J.U. (2018). TRIM56-mediated monoubiquitination of cGAS for cytosolic DNA sensing. Nat. Commun. *9*, 613.

Sliter, D.A., Martinez, J., Hao, L., Chen, X., Sun, N., Fischer, T.D., Burman, J.L., Li, Y., Zhang, Z., Narendra, D.P., et al. (2018). Parkin and PINK1 mitigate STING-induced inflammation. Nature *561*, 258–262.

Sun, L., Wu, J., Du, F., Chen, X., and Chen, Z.J. (2013). Cyclic GMP-AMP synthase is a cytosolic DNA sensor that activates the type I interferon pathway. Science *339*, 786–791.

Tan, X., Sun, L., Chen, J., and Chen, Z.J. (2018). Detection of microbial infections through innate immune sensing of nucleic acids. Annu. Rev. Microbiol. *72*, 447–478.

Tao, J., Zhang, X.W., Jin, J., Du, X.X., Lian, T., Yang, J., Zhou, X., Jiang, Z., and Su, X.D. (2017). Nonspecific DNA binding of cGAS N terminus promotes cGAS activation. J. Immunol. *198*, 3627–3636.

Volkman, H.E., Cambier, S., Gray, E.E., and Stetson, D.B. (2019). Tight nuclear tethering of cGAS is essential for preventing autoreactivity. Elife *8*, e47491.

Wang, H., Hu, S., Chen, X., Shi, H., Chen, C., Sun, L., and Chen, Z.J. (2017). cGAS is essential for the antitumor effect of immune checkpoint blockade. Proc. Natl. Acad. Sci. U S A *114*, 1637–1642.

Weir, C., Hudson, A.L., Moon, E., Ross, A., Alexander, M., Peters, L., Langova, V., Clarke, S.J., Pavlakis, N., Davey, R., et al. (2014). Streptavidin: a novel immunostimulant for the selection and delivery of autologous and syngeneic tumor vaccines. Cancer Immunol. Res. *2*, 469–479.

Wu, J.J., Li, W., Shao, Y., Avey, D., Fu, B., Gillen, J., Hand, T., Ma, S., Liu, X., Miley, W., et al. (2015). Inhibition of cGAS DNA sensing by a herpesvirus virion protein. Cell Host Microbe *18*, 333–344.

Xia, P., Ye, B., Wang, S., Zhu, X., Du, Y., Xiong, Z., Tian, Y., and Fan, Z. (2016). Glutamylation of the DNA sensor cGAS regulates its binding and synthase activity in antiviral immunity. Nat. Immunol. *17*, 369–378.

Yang, H., Wang, H., Ren, J., Chen, Q., and Chen, Z.J. (2017). cGAS is essential for cellular senescence. Proc. Natl. Acad. Sci. U S A *114*, E4612–E4620.

Yoh, S.M., Schneider, M., Seifried, J., Soonthornvacharin, S., Akleh, R.E., Olivieri, K.C., De Jesus, P.D., Ruan, C., de Castro, E., Ruiz, P.A., et al. (2015). PQBP1 is a proximal sensor of the cGAS-dependent innate response to HIV-1. Cell *161*, 1293–1305.

Zempleni, J., Wijeratne, S.S., and Hassan, Y.I. (2009). Biotin. Biofactors *35*, 36–46.

Zhang, X., Shi, H., Wu, J., Zhang, X., Sun, L., Chen, C., and Chen, Z.J. (2013). Cyclic GMP-AMP containing mixed phosphodiester linkages is an endogenous high-affinity ligand for STING. Mol. Cell *51*, 226–235.

iScience, Volume *23*

Supplemental Information

Streptavidin Promotes DNA Binding and Activation of cGAS to Enhance Innate Immunity

Yanqiong Zhang, Zhe Ma, Ying Wang, Joshua Boyer, Guoxin Ni, Liang Cheng, Siyuan Su, Zhigang Zhang, Zhichuan Zhu, Jiayi Qian, Lishan Su, Qi Zhang, Blossom Damania, and Pengda Liu

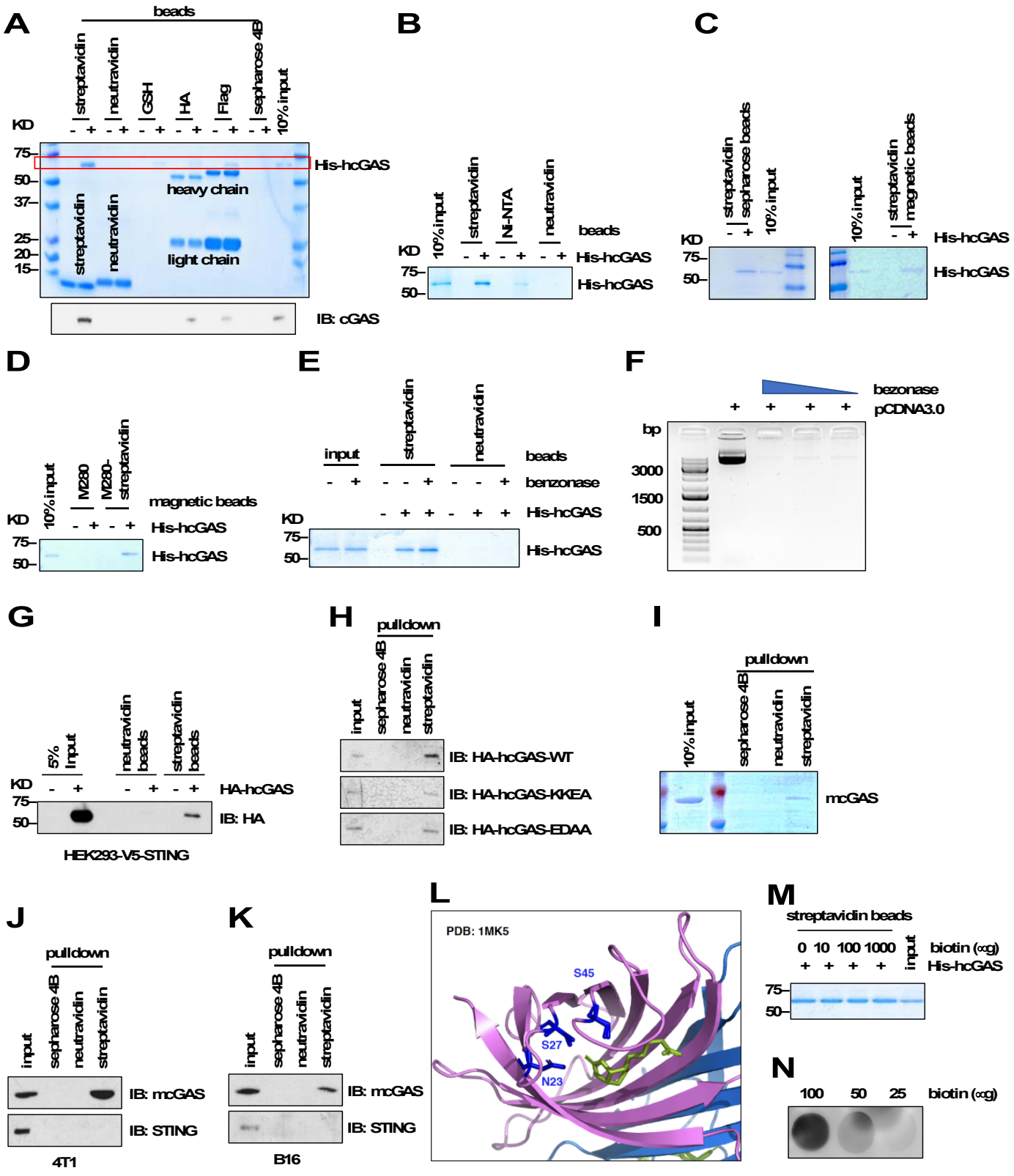
A
beads
streptavidin
neutravidin
GSH
HA
Flag
sepharose 4B
10% input
KD
75
50
37
25
20
15
His-hcGAS
heavy chain
light chain
streptavidin
neutravidin
IB: cGAS
B
10% input
streptavidin
Ni-NTA
neutravidin
beads
KD
75
50
His-hcGAS
His-hcGAS
C
streptavidin
sepharose beads
10% input
10% input
streptavidin
magnetic beads
KD
75
50
His-hcGAS
His-hcGAS
D
10% input
M280
M280-streptavidin
magnetic beads
KD
His-hcGAS
75
50
His-hcGAS
E
input
streptavidin
neutravidin
beads
benzonase
His-hcGAS
KD
75
50
His-hcGAS
F
bezonase
pCDNA3.0
bp
3000
1500
500
G
5% input
neutravidin beads
streptavidin beads
KD
HA-hcGAS
75
50
IB: HA
HEK293-V5-STING
H
pulldown
input
sepharose 4B
neutravidin
streptavidin
IB: HA-hcGAS-WT
IB: HA-hcGAS-KKEA
IB: HA-hcGAS-EDAA
I
pulldown
10% input
sepharose 4B
neutravidin
streptavidin
mcGAS
J
pulldown
input
sepharose 4B
neutravidin
streptavidin
IB: mcGAS
IB: STING
4T1
K
pulldown
input
sepharose 4B
neutravidin
streptavidin
IB: mcGAS
IB: STING
B16
L
PDB: 1MK5
S45
S27
N23
M
streptavidin beads
0 10 100 1000
input
biotin (∞g)
His-hcGAS
75
50
N
100 50 25
biotin (∞g)

Figure S1. Streptavidin binds cGAS *in vitro* and in cells | related to Figure 1.
(A-B) *In vitro* pulldown assays indicated streptavidin beads, but not other agarose beads tested, bind bacterially purified full-length His-hcGAS proteins. **(C-D)** *In vitro* pulldown assays using indicated streptavidin agarose or magnetic beads incubated with bacterially purified full-length His-hcGAS proteins. **(E)** *In vitro* pulldown assays using indicated beads incubated with benzonase treated His-hcGAS proteins. **(F)** Treatment of 3 μg pCDNA3.0 plasmid *in vitro* with increasing amount of benzonase (1, 2 and 4 μL). **(G)** Pulldown assays using indicated beads with WCL derived from HEK293-V5-STING cells transfected with HA-hcGAS constructs. **(H)** Pulldown assays using indicated beads with WCL derived from HEK293T cells transfected with indicated HA-hcGAS constructs. KKEA (K173E/R176E/K407E/K411A) is a hcGAS mutant deficient in binding DNA. EDAA represents E225A/D227A as an enzyme-dead mutant of hcGAS. **(I)** *In vitro* pulldown assays using indicated agarose beads incubated with bacterially purified full-length His-mcGAS proteins. **(J, K)** Pulldown assays using indicated beads with WCL derived from 4T1 (J) or B16 (K) mouse cells. **(L)** A structure model generated by PyMOL2.2.0 using a streptavidin structure from PDB: 1MK5. Biotin binding residues in streptavidin are labeled in blue. Biotin is labeled in green. (**M**) *In vitro* pulldown assays using streptavidin agarose beads with recombinant His-hcGAS proteins with increasing and excess amount of biotin indicate that biotin binding to streptavidin does not significantly affect cGAS binding to streptavidin. (**N**) Dot blot assays for biotin using an anti-biotin antibody.

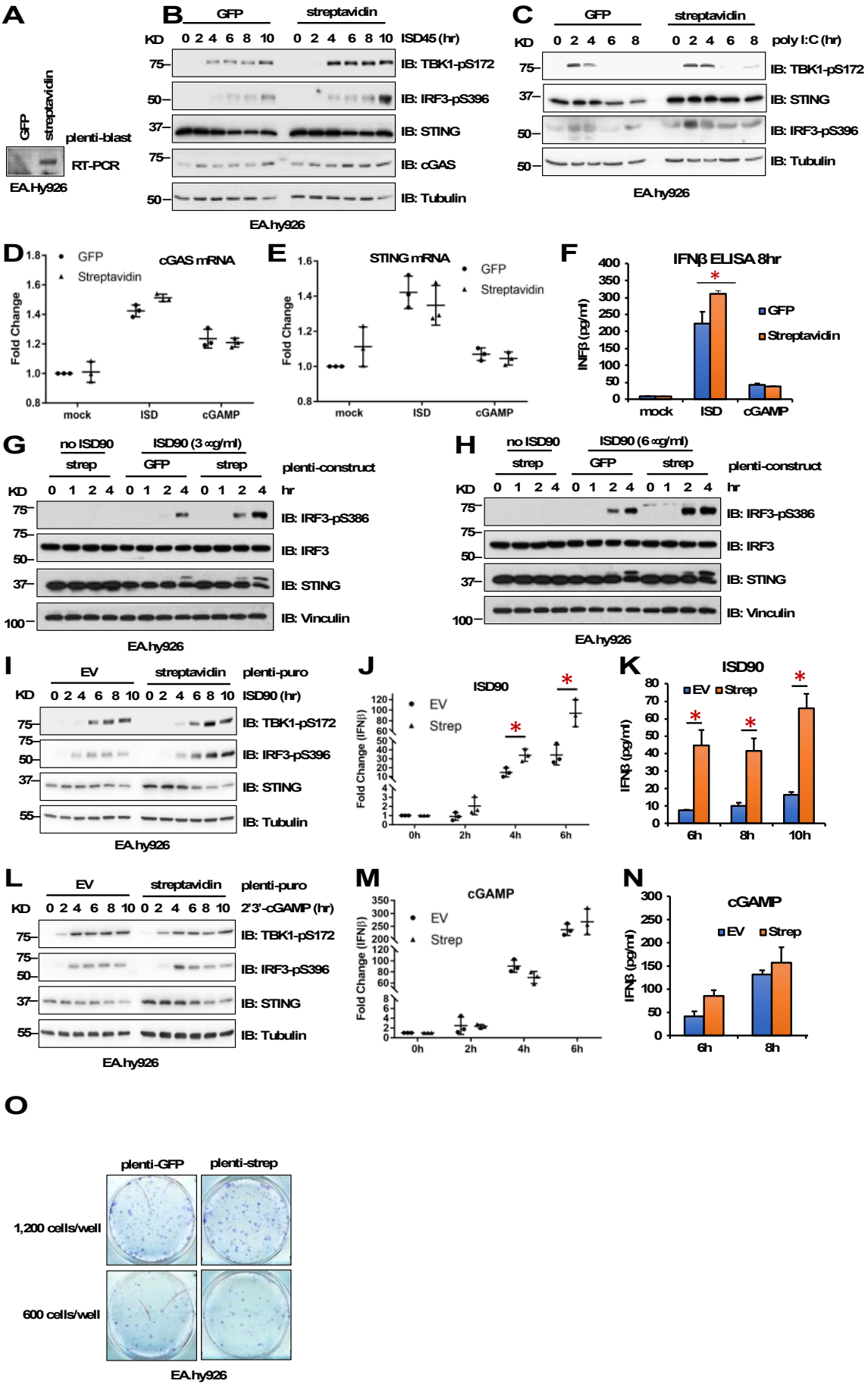
A
GFP
streptavidin
plenti-blast
RT-PCR
EA.Hy926
B
GFP
streptavidin
KD
0 2 4 6 8 10 0 2 4 6 8 10 ISD45 (hr)
75–
IB: TBK1-pS172
50–
IB: IRF3-pS396
37–
IB: STING
75–
IB: cGAS
50–
IB: Tubulin
EA.hy926
C
GFP
streptavidin
KD
0 2 4 6 8 0 2 4 6 8 poly I:C (hr)
75–
IB: TBK1-pS172
37–
IB: STING
50–
IB: IRF3-pS396
50–
IB: Tubulin
EA.hy926
D
GFP
Streptavidin
cGAS mRNA
Fold Change
1.8
1.6
1.4
1.2
1.0
0.8
mock
ISD
cGAMP
E
STING mRNA
GFP
Streptavidin
Fold Change
1.6
1.4
1.2
1.0
0.8
mock
ISD
cGAMP
F
IFNβ ELISA 8hr
*
INFβ (pg/ml)
400
350
300
250
200
150
100
50
0
GFP
Streptavidin
mock
ISD
cGAMP
G
no ISD90
ISD90 (3 ∝g/ml)
strep
GFP
strep
plenti-construct
KD
0 1 2 4 0 1 2 4 0 1 2 4 hr
75–
IB: IRF3-pS386
75–
IB: IRF3
50–
37–
IB: STING
100–
IB: Vinculin
EA.hy926
H
no ISD90
ISD90 (6 ∝g/ml)
strep
GFP
strep
plenti-construct
KD
0 1 2 4 0 1 2 4 0 1 2 4 hr
75–
IB: IRF3-pS386
75–
IB: IRF3
50–
37–
IB: STING
100–
IB: Vinculin
EA.hy926
I
EV
streptavidin
plenti-puro
KD
0 2 4 6 8 10 0 2 4 6 8 10 ISD90 (hr)
75–
IB: TBK1-pS172
75–
50–
IB: IRF3-pS396
37–
IB: STING
55–
IB: Tubulin
EA.hy926
J
ISD90
EV
Strep
Fold Change (IFNβ)
120
100
80
60
50
40
30
20
10
4
3
2
1
0
*
*
0h
2h
4h
6h
K
ISD90
EV
Strep
IFNβ (pg/ml)
80
70
60
50
40
30
20
10
0
*
*
*
6h
8h
10h
L
EV
streptavidin
plenti-puro
KD
0 2 4 6 8 10 0 2 4 6 8 10 2'3'-cGAMP (hr)
75–
IB: TBK1-pS172
75–
50–
IB: IRF3-pS396
37–
IB: STING
55–
IB: Tubulin
EA.hy926
M
cGAMP
EV
Strep
Fold Change (IFNβ)
350
300
250
200
120
100
80
60
8
6
4
2
0
0h
2h
4h
6h
N
cGAMP
EV
Strep
IFNβ (pg/ml)
300
250
200
150
100
50
0
6h
8h
O
plenti-GFP
plenti-strep
1,200 cells/well
600 cells/well
EA.hy926

Figure S2. Streptavidin facilitates DNA-induced cGAS activation | related to Figure 2.
(A) RT-PCR analysis indicating streptavidin is stably expressed in EA.hy926 cells. **(B, C)** IB analyses of WCL derived from control (GFP expressing) or streptavidin expressing EA.hy926 cells transfected with 5 μg/mL ISD45 (B) or 5 μg/mL poly I:C for indicated periods before cell collection. **(D, E)** RT-PCR analyses of cGAS and STING mRNA levels in either GFP or streptavidin expressing EA.hy926 cells treated with ISD45 or cGAMP for 8 hours. **(F)** ELISA analyses of extra-cellular IFNβ levels from either GFP or streptavidin expressing EA.hy926 cells treated with ISD45 or cGAMP for 8 hours. **(G, H)** IB analyses of WCL derived from EA.hy926 cells stably expressing GFP or streptavidin transfected with indicated concentrations of ISD90. Cells were collected at indicated time periods post-ISD90 transfection. **(I, L)** IB analysis of WCL derived from indicated EA.hy926 cells expressing either EV or streptavidin treated with 2 μg/mL ISD90 (I) or 5 μg/mL cGAMP (L) for indicated periods. **(J, M)** RT-PCR analyses of IFNβ mRNA levels from (I) and (L) at the indicated times. **(K, N)** ELISA analyses of IFNβ protein levels from (I) and (L) at indicated periods. **(O)** Representative colony formation assay results by plating indicated number of EA.hy926 cells stably expressing either GFP or streptavidin on 6-well plates. Triplicates were performed, and colonies were stained 14 days post-cell plating.

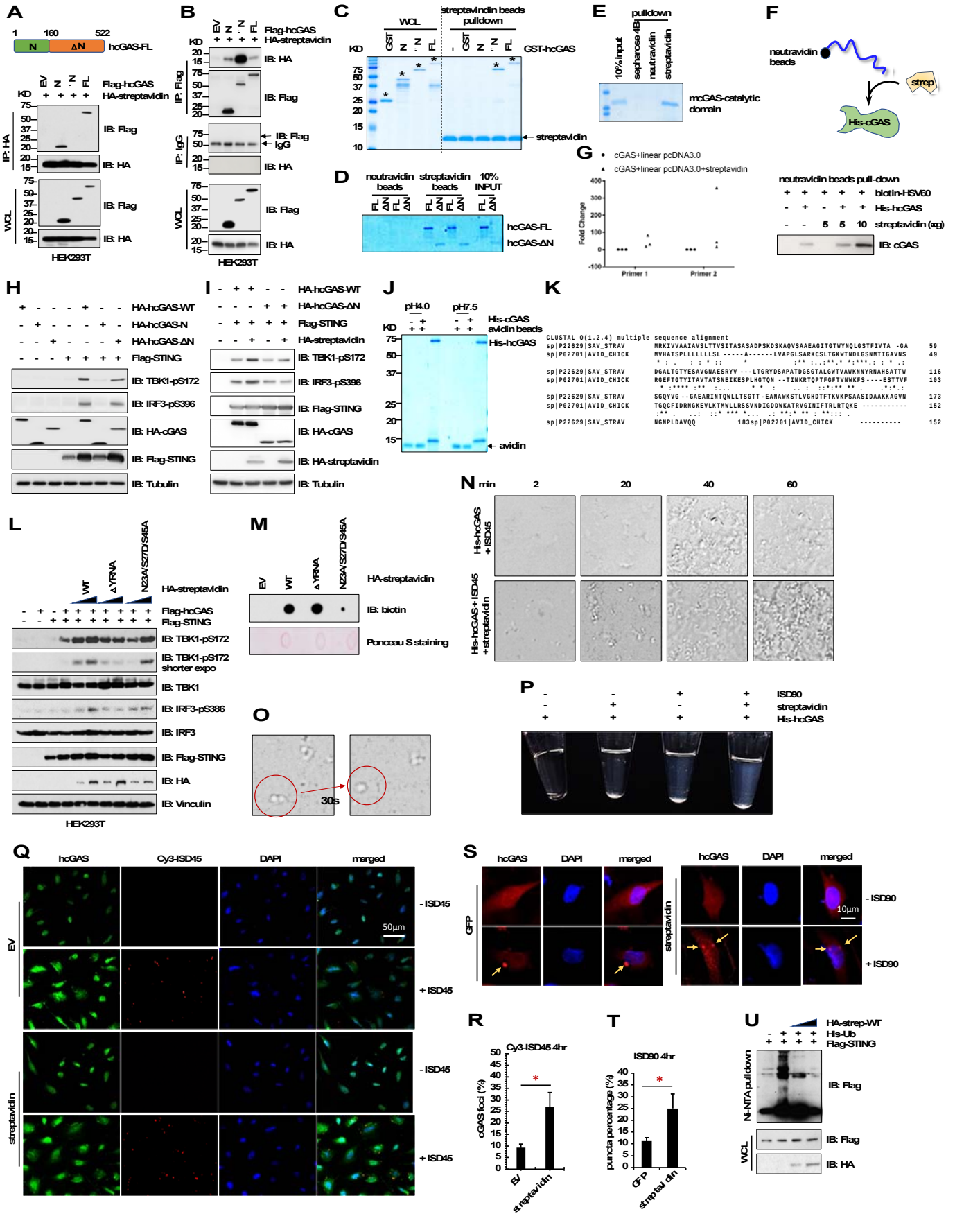
A
1
160
522
N
ΔN
hcGAS-FL
EV
Z
Z
FL
Flag-hcGAS
HA-streptavidin
KD
IP: HA
IB: Flag
IB: HA
WCL
IB: Flag
IB: HA
HEK293T
B
Flag-hcGAS
HA-streptavidin
IP: Flag
IB: HA
IB: Flag
IP: IgG
IB: Flag
IgG
IB: HA
WCL
IB: Flag
IB: HA
HEK293T
C
WCL
streptavindin beads pulldown
GST
GST-hcGAS
streptavidin
D
neutravidin beads
streptavidin beads
10% INPUT
FL
ΔN
hcGAS-FL
hcGAS-ΔN
E
pulldown
10% input
sepharose 4B
neutravidin
streptavidin
mcGAS-catalytic domain
F
neutravidin beads
strep
His-cGAS
G
cGAS+linear pcDNA3.0
cGAS+linear pcDNA3.0+streptavidin
Fold Change
Primer 1
Primer 2
neutravidin beads pull-down
biotin-HSV60
His-hcGAS
streptavidin (∝g)
IB: cGAS
H
HA-hcGAS-WT
HA-hcGAS-N
HA-hcGAS-ΔN
Flag-STING
IB: TBK1-pS172
IB: IRF3-pS396
IB: HA-cGAS
IB: Flag-STING
IB: Tubulin
I
HA-hcGAS-WT
HA-hcGAS-ΔN
Flag-STING
HA-streptavidin
IB: TBK1-pS172
IB: IRF3-pS396
IB: Flag-STING
IB: HA-cGAS
IB: HA-streptavidin
IB: Tubulin
J
pH4.0
pH7.5
His-cGAS
avidin beads
KD
His-hcGAS
avidin
K
CLUSTAL O(1.2.4) multiple sequence alignment
sp|P22629|SAV_STRAV
sp|P02701|AVID_CHICK
L
WT
ΔYRNA
N23A/S27D/S45A
HA-streptavidin
Flag-hcGAS
Flag-STING
IB: TBK1-pS172
IB: TBK1-pS172 shorter expo
IB: TBK1
IB: IRF3-pS386
IB: IRF3
IB: Flag-STING
IB: HA
IB: Vinculin
HEK293T
M
EV
WT
ΔYRNA
N23A/S27D/S45A
HA-streptavidin
IB: biotin
Ponceau S staining
N
min
2
20
40
60
His-hcGAS + ISD45
His-hcGAS + ISD45 +streptavidin
O
30s
P
ISD90
streptavidin
His-hcGAS
Q
hcGAS
Cy3-ISD45
DAPI
merged
EV
streptavidin
- ISD45
+ ISD45
50μm
S
hcGAS
DAPI
merged
GFP
streptavidin
- ISD90
+ ISD90
10μm
R
Cy3-ISD45 4hr
cGAS foci (%)
EV
streptavidin
T
ISD90 4hr
puncta percentage (%)
GFP
streptavidin
U
HA-strep-WT
His-Ub
Flag-STING
Ni-NTA pulldown
IB: Flag
WCL
IB: Flag
IB: HA

Figure S3. Streptavidin binds cGAS to facilitate DNA binding | related to Figure 3.
(A-B) IB analyses of IPs and WCL derived from HEK293T cells transfected with indicated DNA constructs. **(C-D)** Indicated streptavidin beads were incubated with indicated recombinant GST-hcGAS proteins *in vitro* at 4°C for 8 hrs for pulldown assays. **(E)** Indicated beads were incubated with 10 μg mcGAS catalytic domain only proteins *in vitro* for pulldown assays. **(F)** *In vitro* biotin-DNA pulldown assays indicating that addition of recombinant streptavidin proteins promotes DNA binding to recombinant His-cGAS proteins. **(G)** qPCR analyses of DNA obtained from GST-hcGAS pulldown assays as in Figure 3A. **(H-I)** IB analyses of WCL derived from HEK293T cells transfected with indicated DNA constructs. 48 hrs post-transfection, cells were lysed in EBC buffer and subjected to SDS-PAGE analyses. (**J**) Avidin agarose beads pulldown assays indicating avidin does not bind His-cGAS proteins neither at pH4.0 nor at pH7.5 *in vitro*. (**K**) Streptavidin and avidin protein sequence alignment. **(L)** IB analyses of WCL derived from HEK293T cells transfected with indicated DNA constructs. 48 hrs post-transfection, cells were lysed in EBC buffer and subjected to SDS-PAGE analyses. **(M)** YRNA-deleted streptavidin retains its ability to bind biotin. Indicated HA-streptavidin constructs were transfected into HEK293T cells and 48 hrs post-transfection, HA-IPs were performed and washed thoroughly to collect indicated HA-streptavidin proteins on agarose beads. Then these streptavidin-containing agarose beads were incubated with biotin-H3 (21-44) peptides (Anaspec) at 4 °C for 4 hrs before washed with EBC buffer to eliminate non-specific binding proteins. Resulting products were diluted and loaded on nitro-cellulose membrane for both ponceau S staining and western blotting by an anti-biotin antibody (Cell Signaling Technology #5597). **(N)** Representative images for cGAS *in vitro* phase transition processes by incubating indicated materials for indicated time periods *in vitro*. Please refer to the Method for experimental details. **(O)** A representative image for the fusion of cGAS/DNA droplet, a process occurs in 30s. **(P)** *In vitro* phase transition assays indicating that streptavidin facilitates DNA-induced cGAS phase transition. Please refer to Method for details. **(Q, S)** Representative images for cGAS/DNA/streptavidin puncta formation in control or streptavidin expressing EA.hy926 cells. Where indicated, ISD45 (Q) or ISD90 (S) were transfected into indicated cells and cells were fixed 4 hrs post-ISD transfection and subjected to cGAS staining. Scale bars represent 50 μm (Q) and 10 μm (S), respectively. **(R, T)** Quantifications of cGAS foci in (Q) and (S). **(U)** In-cell His-ubiquitination assays by transfecting indicated DNA constructs into HEK293T cells. 48 hrs post-transfections, cells were lysed for his-ubiquitination assays under denatured conditions.

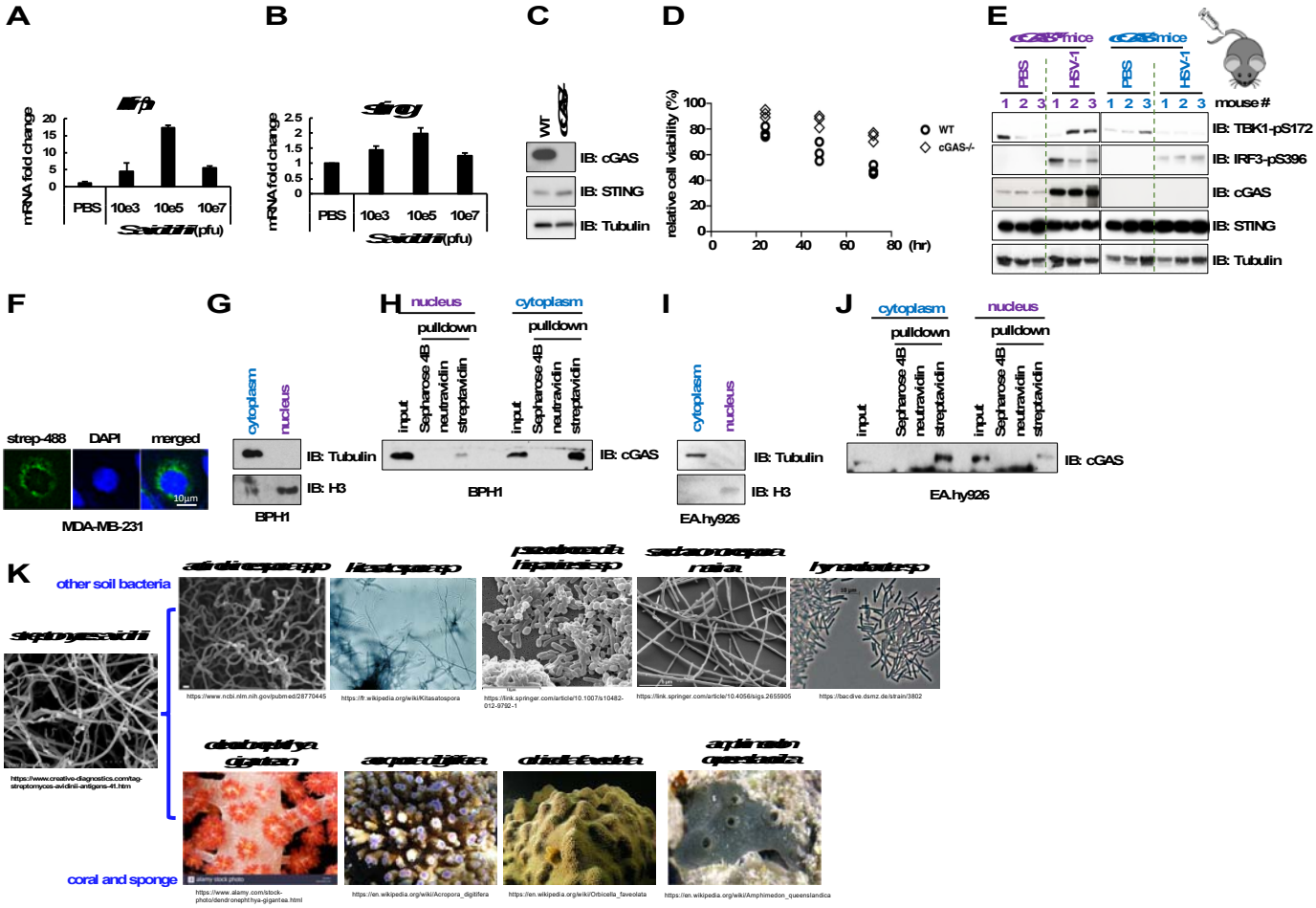

L

```
uncharacterized protein LOC114531979 [ Dendronephthya gigantea]
Sequence ID: XP_028409375.1

strep  45   WYNQLGSTFIVTA--GADGALTGTYESAVGNAESRYVLTGRYDSAPATDGSGTALGWTVA  102
            WYN+LGS  I+T+   +G+  GTY S VG AE  Y L GR+D+      +G+ +GW V+
sbjct  56   WYNELGSEMIITSLDRNNGSFEGTYNSGVGQAEKEYYLVGRFDT ------NGSTIGWVVS  109

strep  103  WKNNYRNAHSATTWSGQ--YVGGAEARINTQWLLTSGTTEANAWKSTLVGHDTFTKVKPS  160
            W+N +  +HS T WSGQ  +    + I T WLLT  T   + W+ST+VG DTFT+  PS
Sbjct  110  WQNKFLISHSTTAWSGQMQFQNPEKPVILTTWLLTRQTEPKDDWESTIVGFDTFTQDPPS  169

strep  161  AASIDAAK  168
              +I+ AK
Sbjct  170  QETIERAK  177

PREDICTED: avidin-related protein 4/5-like, partial [Acropora digitifera]
Sequence ID: XP_015763687.1

strep  41   ITGTWYNQLGSTFIVTAGADGALTGTYESA-------VGNAESRYVLTGRYDSAPATDGS  93
            + G WYNQLGS   +  G+DG L G Y +A        G++ S  V T  YD
Sbjct  31   LDGKWYNQLGSELYLKHGSDGMLLGEYRTAQERFNGSAGSSHSIVVGTAPYDHP ------  84

strep  94   GTALGWTVAWKNNYRNAHSATTWSGQYVGGAEAR--INTQWLLTSGT-TEANAWKSTLVG  150
            GT+  ++V W     RN  S T W+GQ +  ++      + T WLL S    T  + WKST++G
Sbjct  85   GTSFAFSVVW----RNGSSTTIWTGQCLVCSDGHETLLTSWLLRSKVNTCIDKWKSTMIG  140

strep  151  HDTFTKV-------KPSAASIDAAK  168
              DTFT+         KP   S D ++
Sbjct  141  RDTFTRFEQRPGPRKPGNNSTDTSR  165


uncharacterized protein LOC110048043 [ Orbicella faveolata]
Sequence ID: XP_020609468.1

strep  41   ITGTWYNQLGSTFIVTAGADGALTGTYESAV----GNA-ESRYVLTGRYDSAPATDGSGT  95
            + G WYNQLGS   +    DG L G Y +AV    G+A E+  +L G   +AP  D  G
Sbjct  31   LDGKWYNQLGSEIFLKHENDGRLLGEYRTAVERQNGSAGETHSILLG ---TAPY-DYPGA  86
strep  96   ALGWTVAWKNNYRNAHSATTWSGQYV--GGAEARINTQWLLTSGT-TEANAWKSTLVGHD  152
            A  ++V W    RN  S T W+GQ +       ++ T WLL S   T  + W+ST +G D
Sbjct  87   AFAFSVVW----RNGSSTTVWTGQCLVCEDGHEKLLTSWLLRSKVDTCIDKWQSTRIGRD  142
strep  153  TFTKVKPSAASIDAAKKAGVNN  174
            TFT+ +     D  +K  V N
Sbjct  143  TFTRYEQR----DGPRKPDVTN  160

PREDICTED: uncharacterized protein LOC109583125 [ Amphimedon queenslandica]
Sequence ID: XP_019853878.1

strep  26   PSKDSKAQVSAAEAGITGTWYNQLGSTFIVTAG--ADGALTGTYESAVGNAESRYVLTGR  83
            P  DSK Q S     + G W N+LGS   ++A    A+G + G Y S VG+A   Y L G
Sbjct  75   PKIDSKLQTSTVPTSLAGVWTNELGSKMFISASSYAEGQINGLYCSKVGDAYDYYDLNGL  134

strep  84   YDSAPATDGSGTA--LGWTVAWKNNYR-NAHSATTWSGQ-YVGGAEARINTQWLLTSGTT  139
            YD    TDG  T+  LGWTV W N    N+ S T WSGQ Y    +  I T WLL S  T
Sbjct  135  YD----TDGDETSGTLGWTVQWNNGPNGNSQSNTAWSGQRYEISGKLYIYTTWLLVSQET  190

strep  140  EANAWKSTLVGHDTFTK  156
              N W+STL G D F K
Sbjct  191  LENNWESTLTGKDKFCK  207
```

Figure S4. Streptavidin recognizes cGAS *in vitro* and in cells | related to Figure 4.
(A-B) RT-PCR analyses of indicated mRNA levels from mouse spleens 24 hrs post-injection with indicated doses of *Streptomyces avidinii*. **(C)** IB analyses of WCL derived from WT and *cGAS*$^{-/-}$ MDA-MB-231 cells. **(D)** Cell viability assay in the co-culture model as in Figure 4B-4C. Specifically, 10e7 *streptomyces avidinii* bacteria were co-cultured with WT or *cGAS*$^{-/-}$ MDA-MB-231 cells and cells were trypsinized at indicated time periods. 50 μL resuspended cells were mixed with equal volume of trypan blue and cell viability was determined by Biorad TC20 cell counter. **(E)** 10e7 pfu of HSV-1 was injected into BL6 mice through tail vein injection. 4 hrs post-injection, mouse spleens were harvested for IB analyses. **(F)** Representative images of Alexa-488-streptavidin staining of endogenous cGAS in MDA-MB-231 cells. Scale bar represents 10 μm. **(G-J)** IB analyses of WCL or indicated agarose beads pulldowns derived from either BPH1 (G, H) or EA.hy926 (I, J) cells fractionated into either cytoplasmic or nuclear fractions. Please refer to the Method section for experimental details. **(K)** Conservation of streptavidin protein sequence in other streptavidin-like proteins found in bacteria or coral/sponges. **(L)** Protein sequence alignment of streptavidin (labeled as strep) and indicated proteins from coral/sponges.

TRANSPARENT METHODS

KEY RESOURCES TABLE

REAGENT or RESOURCE	SOURCE	IDENTIFIER
Beads and Recombinant Proteins		
Streptavidin sepharose beads	GE Healthcare	cat# 17-5113-01, lot#10261016
Streptavidin magnetic beads	Invitrogen by Thermo Fisher Scientific	cat# 65081D, lot#00723848
Neutravidin agarose beads	Thermo Scientific	cat# 29200, lot#SF252845
Glutathione agarose beads	GE Healthcare	cat# 17-0756-05, lot#10260459
Sepharose 4B beads	Sigma-Aldrich	Product# 4B200
Anti-HA agarose beads	Sigma	cat# A-2095, lot#057M4864V
Anti-Flag agarose beads	Sigma	cat# A2220, lot#SLBW1929
Pierce ™ Avidin agarose beads	Thermo Scientific	cat# 20219, lot#UE284920
Avidin, Egg White	EMD Millipore Corp., USA	cat# 189725, lot# 3185005
Recombinant streptavidin proteins	Chem-Impex International, Inc	cat# 24605, lot#000547-74053
Streptavidin-Gold from Streptomyces avidinii,20 nm particle size	Sigma-Aldrich	cat# 53134-1ML
Dynabeads M-280 sheep anti-Rabbit IgG	Invitrogen	cat# 11204D, lot# 00764095
Dynabeads M-280 Streptavidin	Invitrogen	cat# 11205D, lot# 55750830
Nucleotide stimulants		
ISD45	IDT	5'-TACAGATCTACTAGTGATCTATGACTGATCTGTA CATGATCTACA-3'
ISD90	Eurofins Genomics	5'-TACAGATCTACTAGTGATCTATGACTGATCTG TACATGATCTACATACAGATCTACTAGTGATC TATGACTGATCTGTACATGATCTACA-3'
2’3’-cGAMP	InvivoGen	cat# tlrl-nacga23-02
Antibodies		
Anti-cGAS antibody	Cell Signaling Technology	cat#15102, lot#3
Anti-STING antibody	Cell Signaling Technology	cat#13647, lot#1

Anti-phospho-Ser172-TBK1 antibody	Cell Signaling Technology	cat#5483, lot1#1
Anti-phospho-Ser396-IRF3 antibody	Cell Signaling Technology	cat#29047, lot#1
Anti-phospho-Ser386-IRF3 antibody	Cell Signaling Technology	cat#37829, lot#1
Anti-HA antibody	Cell Signaling Technology	cat#3724, lot#8
Polyclonal anti-Flag antibody	Sigma	cat#F-7425, lot#078M4886V
Monoclonal anti-Flag antibody	Sigma	cat#F-3165, clone M2, lot#SLBN8915V
Monoclonal anti-Tubulin antibody	Sigma	cat#T-5168, lot#115M4828V
Peroxidase-conjugated anti-mouse secondary antibody	Sigma	cat#A-4416, lot#SLBW4917
Peroxidase-conjugated anti-rabbit secondary antibody	Sigma	cat#A-4914, lot#SLBV6850
Goat anti-Rabbit IgG (H+L) Secondary Antibody, Rhodamine	Invitrogen	cat# 31670
Fluor-488-streptavidin probe	Invitrogen	cat#21832, lot#T1262799
Transfection Reagents and Antibiotics		
Lipofectamine 3000	Invitrogen by Thermo Fisher Scientific	cat# L3000150
Lipofectamine 2000	Invitrogen by Thermo Fisher Scientific	cat# 11668500
Polyethylenimine (PEI)	Polysciences, Inc.	cat# 23866-1, lot# 690174
Puromycin	Fisher BioReagents	cat# 58-58-2, lot# 184968
Blasticidin	Fisher BioReagents	cat# 3513-03-9, lot# 171370
Experimental Models: Cell Lines		
HEK293	Dr. Wenyi Wei (BIDMC, HMS)	
HEK293T	Dr. Qing Zhang (UT-Southwestern Medical Center)	
HEK293-V5-STING	Dr. Blossom Damania (UNC)	
MDA-MB-231	(UT-Southwestern Medical Center)	
EA.hy926	Dr. Blossom Damania (UNC)	
Software		

Origin7 (Microcal)	OriginLab Corporation	https://microcal-origin.joydownload.com/
SPSS Statistics	IBM Corporation	SPSS 11.5 Statistical Software
Others		
Rneasy Mini Kit	QIAGEN	cat# 74106
iScript™ Reverse Transcription Supermix for RT-qPCR	Bio-Rad	cat# 170-8891
PowerUp™ SYBR™ Green Master Mix	Appliedbiosystems by Thermo Fisher Scientific	cat# A25742, lot# 00718807
ELISA kit	R&D systems	cat# DY814-05, lot#P181016
Protease Inhibitor Cocktail	Bimake	cat# B14012, lot# 411013
Phosphatase inhibitor cocktail A and B	Bimake	cat# B15001-A /B15001-B, lot# 510028
ProLong™ Gold Antifade Mountant with DAPI	Invitrogen	cat# P36931, lot#1926936
GelCode™ Blue Stain Reagent	Thermo Scientific	cat# 24592, lot# SF252345
Deposited Data		
Original microscope images and uncropped western blot images can be found at the DOI URL:		

METHOD DETAILS

Cell Culture

HEK293, HEK293T, MDA-MB231 and EA.hy926 cells were cultured in DMEM supplemented with 10% fetal bovine serum, 100 units of penicillin and 100 mg/ml streptomycin at 37 °C with 5% CO_2.

Transfection and Lentiviral Production

Cell transfection was performed using lipofectamine 3000, 2000 (Invitrogen) or polyethylenimine (PEI) (Polysciences), as described previously (Jiang et al., 2019; Liu et al., 2014; Liu et al., 2015a). Packaging of lentiviral sgRNA or cDNA expressing viruses, as well as subsequent infection of EA.hy926 cells were performed according to the protocols described previously (Guo et al., 2016; Liu et al., 2015b). Following viral infection, cells were maintained in the presence of hygromycin (200 μg/ml), puromycin (1 μg/ml) or blasticidin (5 μg/ml), depending on the viral vector used to infect cells.

Plasmids

His-cGAS, HA-cGAS and Flag-cGAS were constructed by cloning cGAS cDNA (PCR by BglII-F and XhoI-R primers) into pET28b, pCDNA3-HA and pCDNA3-Flag vectors, respectively. Flag-STING plasmid was obtained from Dr. Albert Baldwin (UNC). HA-streptavidin was constructed by cloning streptavidin cDNA into pCDNA3-HA vector by BamHI and XhoI sites. pLenti-puro-streptavidin was constructed by cloning streptavidin cDNA into pLenti-CMV-GFP-Puro (658-5) vector (addgene #17448) by BamHI and SalI. pLenti-puro-cGAS-sgRNA was constructed by cloning annealed sgRNA oligos into pLenti-CRISPR-V2 vector cut by BsmBI according to the protocol from Feng Zhang lab
(https://media.addgene.org/cms/files/Zhang_lab_LentiCRISPR_library_protocol.pdf)
Primers for cloning are listed below:
streptavidin-BglII-F: GCAT AGATCT GCTGAAGCTGGTATCACCG
streptavidin-SalI-R: GCAT GTCGAC TTA GGAAGCAGCGGACGG

cGAS-BglII-F: GCATAGATCTCAGCCTTGGCACGGAAAGGC

cGAS-XhoI-R: GCATCTCGAGTCAAAATTCATCAAAAACTGG

cGAS_XhoI_140_R (cGAS-N): GCATCTCGAG TCAGTCCCAGGGCCCG

cGAS_BglII_141_F (cGAS-ΔN): GCATAGATCTGTGCCCAGCCCCG

cGAS_sgRNA_F: CACCGGCACGTGCTCATAGTAGCTCC

cGAS_sgRNA_R: AAACGGAGCTACTATGAGCACGTGCC

streptavidin-delta-YRNA-F: GGACCGTTGCTTGGAAAAACAAC CACTCCGCTACCACCTGG

streptavidin-delta-YRNA-R: CCAGGTGGTAGCGGAGTG GTTGTTTTTCCAAGCAACGGTCC

Immunoblot and Immunoprecipitations Analyses

Cells were lysed in EBC buffer (50 mM Tris pH 7.5, 120 mM NaCl, 0.5% NP-40) or Triton X-100 buffer (50 mM Tris pH 7.5, 150 mM NaCl, 1% Triton X-100) supplemented with protease inhibitors (Complete Mini, Roche) and phosphatase inhibitors (phosphatase inhibitor cocktail set I and II, Calbiochem). The protein concentrations of whole cell lysates were measured by NanoDrop OneC (Thermo Scientific) using the Bio-Rad protein assay reagent as described previously (Liu et al., 2014). Equal amounts of whole cell lysates were resolved by SDS-PAGE and immunoblotted with indicated antibodies. For immunoprecipitations analysis, 1000 μg lysates containing tagged molecules were incubated with agarose beads coupled antibodies for the specific tag for 3-4 hr at 4 °C. The recovered immuno-complexes were washed five times with NETN buffer (20 mM Tris, pH 8.0, 100 mM NaCl, 1 mM EDTA and 0.5% NP-40) before being resolved by SDS-PAGE and immunoblotted with indicated antibodies.

His-cGAS Protein Purification

The recombinant His_6-hcGAS was expressed in *E. coli* BL21with isopropyl β-D-1-thiogalactopyranoside (IPTG) induction 1-2 days at 14ºC. The bacteria pellets were resuspended in lysis buffer (25 mM Tris-Cl pH7.5, 1 M NaCl, 10 μM $ZnCl_2$, 5 mM β-mercaptoethanol, 0.2% NP40, 10% Glycerol, protease inhibitor) and cracked with NanoDeBee homogenizer. At a final concentration of 0.2% PEI (pH7.6) was added to the lysate while stirring for

20 min at 4ºC to precipitate any nucleic acids. Following centrifugation for 40 min at 25000*g* and 4ºC, the supernatant was collected and filtered. The proteins were first purified over a nickel-NTA column with an imidazole gradient. Next, proteins were dialyzed against Ion exchange buffer A (50 mM Tris pH 7.5, 150 mM NaCl, 10 μM $ZnCl_2$, and 5 mM β-mercaptoethanol). Proteins were loaded onto a cation exchange column and eluted with a gradient from 150 mM to 1 M NaCl. Properly folded cGAS proteins were eluted at approximately the 50% mark of the titration with misfolded aggregates titrating at higher concentrations in the gradient. The proteins were concentrated and exchanged into S75 buffer (50 mM Tris pH 7.5, 150 mM NaCl, 10 μM $ZnCl_2$, and 5 mM DTT) with 10K centrifugal filters (Amicon Ultra). Finally, proteins were passed through a S75 size exclusion column to remove any remaining degradation products. Proteins generated via this protocol were deemed >95% pure determined by SDS-PAGE.

In vitro Pulldown Assays

10 μL of indicated agarose or magnetic beads were incubated with 5 μg of recombinant His-hcGAS proteins in a total volume of 500 μl NETN buffer (Jiang et al., 2019; Liu et al., 2014; Liu et al., 2015a) for 4 hrs at 4°C. The agarose or magnetic beads were washed four times with NETN buffer. Bound proteins were eluted by boiling in SDS loading buffer and resolved by SDS-PAGE for subsequent staining by GelCode™ Blue (Thermo Fisher Scientific) or for western blotting.

Cell Fractionation

4x10 cm dishes of confluent cells were trpsinized, washed with ice-cold PBS and collected by centrifugation at 4 ºC at 1,000 rpm for 3 min. Cell pellets were resuspended in 1 mL hypotonic buffer (10 mM HEPES, pH7.9, 1.5 mM MgCl2, 10 mM KCl, 0.5 mM DTT with protease inhibitor) and transferred to a prechilled 1 mL dounce homogenizer. Cells were lysed using 10 strokes of a tight pestle. Resulting products were incubated on ice for 5 min and cell plasma membrane lysis was confirmed by microscopy before moving to next steps. Cells were centrifuged at 1,000 rpm at 4 ºC for 10 min and supernatant was collected as “cytoplasmic” fraction. Cell pellets were thoroughly washed with large volumes of ice-cold PBS and resuspended in hypotonic buffer and subjected

to sonication. Cell debris were spin down at 1,000 rpm at 4 ºC for 10 min and supernatant was collected as "nuclear" fraction.

Isothermal Titration Calorimetry (ITC)

ITC measurements were performed using a MicroCal auto-iTC200 calorimeter (MicroCal, LLC). Purified human His-tagged full-length cGAS was dialyzed against 50 mM HEPES buffer (pH 7.2) with 100 mM NaCl and 0.1mM TCEP for overnight at 4 °C. The concentration of the protein was measured using Pierce® BCA protein assay. The ITC assay was carried out at 25°C. The dialyzed His-cGAS was diluted to 10 µM in the dialysis buffer. Then, 2 µl of streptavidin 100 µM, dissolved in the same dialysis buffer, were injected into 0.2 ml of His-cGAS protein in the chamber for every 180s. The dissociation constants and thermodynamic parameters were determined by using the embedded software package Origin7 (Microcal).

Immunofluorescence and Confocal Analysis

Cells were grown on glass coverslips for 24 hours and fixed with 4% formaldehyde in 1xPBS for 10 minutes at room temperature and permeabilized with 0.1% Triton X-100 in 1x PBS for 10 minutes. Samples were rinsed three times in 1x PBST with 5 minutes each wash. Coverslips were then blocked for 30 minutes with 10% BSA and incubated with either cGAS primary antibody (Cell Signaling Technology cat#15102) or indicated FITC-streptavidin or avidin probes for 60-120 minutes. After 3 x 5 minute, 1x PBST (0.1% Tween-20) washes, the coverslips were incubated with goat anti rabbit IgG (H+L) secondary antibody (Rhodamine Red, Invitrogen) for 60 minutes (for cGAS antibody staining only) and washed three times with 1x PBST. Coverslips were rinsed 3 x 5 minutes with 1x PBS and mounted onto slides using prolong gold anti-fade reagent containing 4,6-diamidino-2-phenylindole (DAPI) (Invitrogen cat#D1306). Pictures were taken using a Keyence BZ-X700 microscope.

In vitro Phase Transition Assays

For the *in vitro* phase transition assays in Figure S3P, purified His-cGAS proteins (5 μg) were mixed with ISD90 (5 μg) only, streptavidin (10 μg) only or both in 200 μL PCR tubes. The total solution volume is 60 μl for all reactions. After 20 min incubation at room temperature, the transparency of solutions were imaged by camera.

For the *in vitro* phase transition assays in Figure S3N-S3O, recombinant His-cGAS proteins (6 μg) was mixed with ISD45 in 96-well plates coated with 20 mg/ml BSA in μl buffer composed of 20 mM Tris-HCl, pH7.5, 150 mM NaCl and 1 mg/ml BSA. Mixtures were incubated at room temperature and images were captured using 40x lens on an Invitrogen EVOS XL Core microscope at indicated time. This method is adapted from (Du and Chen, 2018).

RT-PCR

RT-PCR primers for detection of IFN□, cGAS and STING are as below:

hIFNβ-F: 5'-TCTCCTCCAAATTGCTCTCC-3'

hIFNβ-R: 5'-CTCCCATTCAATTGCCACAG-3'

hcGAS-F: 5'-TAACCCTGGCTTTGGAATCA-3'

hcGAS-R: 5'-TAGCCGCCATGTTTCTTCTT-3'

hSTING-F: 5'-GAGCAGGCCAAACTCTTCTG-3'

hSTING-R: 5'-TGCCCACAGTAACCTCTTCC-3'

hβ-actin-F: 5'-CCTGGCACCCAGCACAAT-3'

hβ-actin-R: 5'-GCCGATCCACACGGAGTA-3'

mIFNβ-F: 5'-GCTCCAAGAAAGGACGAACA-3'

mIFNβ-R: 5'-CATCTCTTGGATGGCAAAGG-3'

mβ-actin-F: 5'-TACCACAGGCATTGTGATGG-3'

mβ-actin-R: 5'-TCTCAGCTGTGGTGGTGAAG-3'

HSV-1 ICP27-F: 5'-GCGTCCTTCGTGTTTGTCATT-3'

HSV-1 ICP27-R: 5'-GCATCTTCTCTCCGACCCCG-3'

RT-PCR experiments were performed as below: Total cellular RNA was extracted using RNeasy mini kit (QIAGEN) according to the manufacturer's protocol and quantified by a spectrophotometer (Nanodrop OneC, Thermo Scientific). cDNA was synthesized using iScript^{TM} Reverse Transcription Supermix for RT-qPCR (Bio-Rad Cat#1708841). cDNA templates and iTaq^{TM} universal SYBR Green Supermix (Bio-rad Cat#1725122) were mixed together and the RT-PCR reaction was performed on the ViiA^{TM}6 Real-Time PCR system. The expression of INFβ, cGAS and STING mRNAs was normalized to the expression of β-actin.

ELISA

ELISAs for human IFN-β were performed using supernatants from cells in which values are expressed as pg/ml ± SD as calculated from a standard curve derived from recombinant IFN-β provided in the ELISA kit (R&D systems, cat# DY814-05, lot#P181016).

HSV-1 Genomic DNA Copy Number

Genomic DNA was extracted from cells and mouse brains using DNeasy Blood & Tissue Kit (Qiagen) according to manufacturer's protocol. HSV-1 genomic DNA copy numbers were then determined by the following HSV-1 specific real-time PCR primers: Forward 5'- CATCACCGACCCGGAGAGGGAC-3', Reverse 5'-GGGCCAGGCGCTTGTTGGTGTA-3'.

HSV-1 Infection Mouse Model

4-8 week-old C57BL/6 WT and *cGAS*$^{-/-}$ mice were purchased from The Jackson Laboratory (stock no. 026554). 100 μL of HSV-1 viruses with indicated pfu were injected into indicated mice through tail vein injection. Where indicated, 100 μL of streptavidin nanoparticles were also injected into indicated mice through tail vein injection. 24 hours post-infection, spleen and brain tissues were harvested and indicated signals were analyzed.

QUANTIFICATION AND STATISTICAL ANALYSIS

Statistics

Differences between control and experimental conditions were evaluated by Student's *t* test or One-way ANOVA. These analyses were performed using the SPSS 11.5 Statistical Software and $P \leq 0.05$ was considered statistically significant.

SUPPLEMENTAL REFERENCES

Du, M., and Chen, Z.J. (2018). DNA-induced liquid phase condensation of cGAS activates innate immune signaling. Science *361*, 704-709.

Guo, J., Chakraborty, A.A., Liu, P., Gan, W., Zheng, X., Inuzuka, H., Wang, B., Zhang, J., Zhang, L., Yuan, M., *et al.* (2016). pVHL suppresses kinase activity of Akt in a proline-hydroxylation-dependent manner. Science *353*, 929-932.

Jiang, Y., Zhang, Y., Leung, J.Y., Fan, C., Popov, K.I., Su, S., Qian, J., Wang, X., Holtzhausen, A., Ubil, E., *et al.* (2019). MERTK mediated novel site Akt phosphorylation alleviates SAV1 suppression. Nat Commun *10*, 1515.

Liu, P., Begley, M., Michowski, W., Inuzuka, H., Ginzberg, M., Gao, D., Tsou, P., Gan, W., Papa, A., Kim, B.M., *et al.* (2014). Cell-cycle-regulated activation of Akt kinase by phosphorylation at its carboxyl terminus. Nature *508*, 541-545.

Liu, P., Gan, W., Chin, Y.R., Ogura, K., Guo, J., Zhang, J., Wang, B., Blenis, J., Cantley, L.C., Toker, A., *et al.* (2015a). PtdIns(3,4,5)P3-Dependent Activation of the mTORC2 Kinase Complex. Cancer Discov 5, 1194-1209.

Liu, P., Gan, W., Guo, C., Xie, A., Gao, D., Guo, J., Zhang, J., Willis, N., Su, A., Asara, J.M., *et al.* (2015b). Akt-mediated phosphorylation of XLF impairs non-homologous end-joining DNA repair. Mol Cell *57*, 648-661.